

Revisiting the Sliced Wasserstein Kernel for Persistence Diagrams: a Figalli–Gigli approach.

Marc Janthial¹ and Théo Lacombe²

¹École polytechnique, Palaiseau, France.

²Laboratoire d’Informatique Gaspard Monge, Univ. Gustave Eiffel, CNRS, LIGM, F-77454, Marne-la-Vallée, France.

Contributing authors: marc.janthial@polytechnique.org;
theo.lacombe@univ-eiffel.fr;

Abstract

The Sliced Wasserstein Kernel (SWK) for persistence diagrams was introduced in (Carrière et al. 2017) as a powerful tool to implicitly embed persistence diagrams in a Hilbert space with reasonable distortion. This kernel is built on the intuition that the Figalli–Gigli distance—that is the partial matching distance routinely used to compare persistence diagrams—resembles the Wasserstein distance used in the optimal transport literature, and that the later could be sliced to define a positive definite kernel on the space of persistence diagrams. This efficient construction nonetheless relies on ad-hoc tweaks on the Wasserstein distance to account for the peculiar geometry of the space of persistence diagrams.

In this work, we propose to revisit this idea by directly using the Figalli–Gigli distance instead of the Wasserstein one as the building block of our kernel. On the theoretical side, our sliced Figalli–Gigli kernel (SFGK) shares most of the important properties of the SWK of Carrière et al., including distortion results on the induced embedding and its ease of computation, while being more faithful to the natural geometry of persistence diagrams. In particular, it can be directly used to handle infinite persistence diagrams and persistence measures. On the numerical side, we show that the SFGK performs as well as the SWK on benchmark applications.

Keywords: Topological data analysis, Optimal Transport, Sliced Wasserstein distance, Kernel methods

Acknowledgements: Authors thank Clément Bonet for fruitful discussions. The work of TL is supported by the Agence Nationale de la Recherche (ANR) under grant ANR-24-CE23-7711 (project TheATRE). This work was done when MJ was intern at Laboratoire d’Informatique Gaspard Monge (Univ. Gustave Eiffel, CNRS).

1 Introduction

Topological Data Analysis (TDA) is an emerging field in data analysis which aims to design topological descriptors of complex structured objects. Its main tools are built upon persistent homology theory, and the most well-known descriptor it produces is called the persistence diagram (PD). PDs enjoy strong stability properties with respect to perturbation of the data (Chazal et al. 2016), and have found many applications in several fields such as computer graphics (Pascucci et al. 2010; Carrière et al. 2015; Tierny et al. 2017), material science (Hiraoka et al. 2016; Saadatfar et al. 2017; Olejniczak and Tierny 2023), computational biology (Bukkuri et al. 2021; Aukerman et al. 2021; Chung et al. 2024), to name a few. Nevertheless, their use in those applications is not straightforward. Indeed, PDs take the form of point clouds with multiplicities in \mathbb{R}^2 and are typically compared using transport-like metrics (Figalli and Gigli 2010; Divol and Lacombe 2020), which are quite expensive to compute in practice (Peyré and Cuturi 2020). Furthermore, the space of PDs equipped with such metrics is not Hilbert (Turner et al. 2014; Turner and Spreemann 2020; Bubenik and Wagner 2020), preventing their direct use in learning methods which require that structure on the descriptor space (e.g. PCA, SVM). A workaround explored in the literature consists in defining kernels on that space to map PDs to vectors in a (possibly infinite-dimensional) Hilbert space. Several contributions have been made using this approach (Reininghaus et al. 2015; Kusano et al. 2018; Bubenik 2015) by defining an explicit embedding of PDs in a Hilbert space.

Particularly inspiring for this work, Carrière et al. (2017) proposed the *Sliced Wasserstein Kernel* (SWK) based on the *Sliced Wasserstein distance* used in computational optimal transport (Rabin et al. 2011). That distance enjoys important stability properties, is fairly easy to compute and—of crucial importance—is provably conditionally negative definite on the space of finite PDs and can therefore be used to define a (Gaussian or Laplace) kernel on the space of persistence diagrams. Their construction is presented in more details in Section 2.4.2.

Contributions In this work, we introduce a new approach to defining sliced distances on the space of persistence diagrams that remains faithful to its underlying geometry. Building on the framework of Divol and Lacombe (2020), which relies on the Figalli–Gigli metric (Figalli and Gigli 2010)—a variant of the Wasserstein distance specifically designed to account for the distinguished role of the diagonal—we define the *Sliced Figalli–Gigli distance* between persistence diagrams. A key feature of the resulting distance is that, unlike its Sliced Wasserstein counterpart, it naturally extends to infinite persistence diagrams and, more generally, to persistence measures. This places SFG within a broader and more intrinsic geometric framework for comparing topological descriptors, rather than restricting it to the finite-diagram setting. We show that this increased generality does not come at the expense of either theoretical guarantees or computational tractability. In particular, we establish stability results for SFG comparable¹ to those known for the Sliced Wasserstein distance, and

¹and, to some extent, more general as we derive them for any exponent $p \geq 1$ while Carrière et al. (2017) restrict the analysis to $p = 1$.

we propose efficient algorithms for its computation. Our numerical experiments further demonstrate that kernels derived from SFG achieve empirical performance on par with that of the Sliced Wasserstein kernel. Overall, the SFG distance and its associated kernel can be viewed as a principled refinement of the Sliced Wasserstein kernel of [Carrière et al. \(2017\)](#), providing a unified framework that applies to a wider class of persistence-based representations while preserving both theoretical soundness and practical efficiency.

Outline. In Section 2, we introduce the necessary background on persistence diagrams and kernel methods before reviewing related works in the literature. In Section 3 we define the *Sliced Figalli–Gigli* distance and study its theoretical properties. In Section 4, we give algorithms for efficient computation of that new distance and discuss the experimental performances of the resulting kernel in numerical applications.

2 Background

2.1 Persistent homology and persistence diagrams

Persistent homology is a machinery based on algebraic topology used to define stable descriptors of real-valued functions on topological spaces. Persistence diagrams (PDs) are one of the most well-known of these descriptors and they, roughly speaking, encode information about *topological components* (such as loops, connected components, enclosed surfaces...) of the underlying function and topological space (see [\(Edelsbrunner and Harer 2010\)](#) for an introduction).

More precisely, given a topological space X and a function $f : X \rightarrow \mathbb{R}$, define $H_k(t)$ to be the k -th homology group of $X_t := f^{-1}([-\infty, t])$ over an arbitrary field. For $s \leq t$, the inclusion $X_s \hookrightarrow X_t$ induces a map $\iota_{s,t}$ between the homology groups $H_k(s)$ and $H_k(t)$. By functoriality of homology, these maps satisfy that for all $r \leq s \leq t$ the following diagram commutes:

$$\begin{array}{ccc} H_k(r) & \xrightarrow{\iota_{r,t}} & H_k(t) \\ & \searrow \iota_{r,s} & \nearrow \iota_{s,t} \\ & H_k(s) & \end{array} \quad (1)$$

The collection of the homology groups $(H_k(t))_{t \in \mathbb{R}}$ along with the maps $(\iota_{s,t})_{s,t \in \mathbb{R}}$ satisfying (1) form a *persistence module* M_f . It has been shown [\(Botnan and Crawley-Boevey 2020\)](#) that under general assumptions this persistence module can be uniquely decomposed over a family $(k_I)_{I \subset \mathbb{R}}$ indexed over the intervals of \mathbb{R} . Given the decomposition $M_f := \bigoplus_j k_{I_j}$, the **persistence diagram** D of f is the multiset of the endpoints of the intervals I_j and is therefore a multiset supported on the open half-plane $\Omega := \{(b, d) \in \mathbb{R}^2, b < d\}$. Following [Chazal et al. \(2016\)](#), one may equivalently think of PDs as **locally finite measures supported on Ω of the form** $\sum_x n_x \delta_x$, where δ_x denotes the Dirac mass located at $x \in \Omega$ and $n_x \in \mathbb{N}$ denotes the multiplicity of x . We adopt this perspective in the rest of this work.

A point (b, d) being in D can be interpreted as a k -dimensional homology component appearing (being "born") in X_b and disappearing ("dying") in X_d . As such the

persistence diagram encodes the birth and death of *topological components* (connected component, loop, void ...) at all scales. One of the main advantages of PDs is their stability with respect to perturbation of the data (Chazal et al. 2016) which has motivated their use in several machine learning tasks. The interested reader may refer to (Edelsbrunner and Harer 2010; Oudot 2015) for more comprehensive introductions.

2.2 Distances between persistence diagrams

Treating PDs as locally finite measures supported on Ω , distances between PDs can be built following (Divol and Lacombe 2020), relying on the formalism introduced by Figalli and Gigli (2010). Let $\mathcal{M}(\Omega)$ be the space of non-negative Radon measures supported on Ω , that is the space of non-negative measures μ supported on Ω such that for every compact subset $A \subset \Omega$, one has $\mu(A) < +\infty$. Given $\mu \in \mathcal{M}(\Omega)$, define the p -persistence of μ as

$$\text{Pers}_p(\mu) := \left(\int_{\Omega} d(x, \partial\Omega)^p \mu(x) \right)^{\frac{1}{p}}, \quad (2)$$

where $d(x, \partial\Omega)$ denote the Euclidean distance between a point $x \in \Omega$ and its orthogonal projection onto the diagonal $\partial\Omega := \{b = d\}$. Let the set of measures with finite persistence, called the space of *persistence measures*, be defined as

$$\mathcal{M}^p(\Omega) := \{\mu \in \mathcal{M}(\Omega) : \text{Pers}_p(\mu) < +\infty\}. \quad (3)$$

With this formalism, the set of persistence diagrams $\mathcal{D}(\Omega)$ is the subset of $\mathcal{M}(\Omega)$ consisting of *point measures*, i.e. locally finite Radon measures of the form $\sum_{i \in I} \delta_{x_i}$ where δ_{x_i} denote the Dirac mass at $x_i \in \Omega$, and I is a (possibly countably infinite) set of indices. Let also $\mathcal{D}^p(\Omega) := \mathcal{D}(\Omega) \cap \mathcal{M}^p(\Omega)$. The Figalli–Gigli distance FG_p is then defined on $\mathcal{M}^p(\Omega)$ as:

$$\text{FG}_p(\mu, \nu) := \left(\inf_{\gamma \in \text{Adm}(\mu, \nu)} \iint_{\overline{\Omega} \times \overline{\Omega}} d(x, y)^p d\gamma(x, y) \right)^{\frac{1}{p}}. \quad (\text{FG}_p)$$

where d is again the Euclidean distance² on \mathbb{R}^2 and the set of admissible transport plans $\text{Adm}(\mu, \nu)$ is the set of Radon measures supported on $\overline{\Omega} \times \overline{\Omega}$ satisfying that for all Borel subsets $A, B \subset \Omega$;

$$\gamma(A \times \overline{\Omega}) = \mu(A) \quad \text{and} \quad \gamma(\overline{\Omega} \times B) = \nu(B). \quad (4)$$

Remark 1 This formalism slightly differs from the usual definitions of PD metrics found in the TDA literature, where PDs are encoded as multi-sets on Ω , and for which (FG_p) is replaced by

$$d_p(\mu, \nu) := \left(\inf_{\gamma \in \Gamma(\mu, \nu)} \sum_{x \in \text{spt}(\mu) \cup \partial\Omega} d(x, \gamma(x))^p \right)^{\frac{1}{p}}, \quad (d_p)$$

²Any other q -norm could be used seamlessly for $q > 1$.

where $\Gamma(\mu, \nu)$ is the set of bijections between $\text{spt}(\mu) \cup \partial\Omega$ and $\text{spt}(\nu) \cup \partial\Omega$, where spt denote the support of a point measure where points are counted with multiplicity. [Divol and Lacombe \(2020\)](#) prove that (d_p) and $\text{FG}_p(\mu, \nu)$ coincide when $\mu, \nu \in \mathcal{D}^p(\Omega)$, the latter presenting the advantage of being well-defined on persistence measures, a more general class of objects which proved to be useful in TDA through various works ([Chazal and Divol 2018](#); [Divol and Lacombe 2021](#); [Cao and Monod 2022](#); [Wu et al. 2024](#)).

Remark 2 These distances resemble the Wasserstein distance between probability measures introduced in the optimal transport literature (see ([Santambrogio 2015](#))), defined as

$$W_p(\mu, \nu) = \left(\inf_{\gamma \in \Pi(\mu, \nu)} \iint_{\Omega \times \Omega} d(x, y)^p d\gamma(x, y) \right)^{\frac{1}{p}}, \quad (\text{W}_p)$$

where the set of admissible transport plans $\Pi(\mu, \nu)$ is in this case the set of measures supported on $\Omega \times \Omega$ with marginals μ and ν .

This similarity led the TDA community to refer to (d_p) as the “Wasserstein distance between persistence diagrams” ([Turner et al. 2014](#); [Berwald et al. 2018](#); [Skraba and Turner 2020](#); [Bubenik and Elchesen 2022](#)). We stress that (d_p) nonetheless differs from (W_p) : the Wasserstein distance is a distance between non-negative measures with the *same (finite) total mass*, where the whole mass of a source measure μ must be transported exactly to the target measure ν . In particular, in contrast to (d_p) , (W_p) does not allow one to transport an arbitrary (possibly infinite) amount of mass to and from the diagonal $\partial\Omega$. The Sliced Wasserstein Kernel of Carrière et al. ([Carrière et al. 2017](#)) is built on the actual Wasserstein distance (W_p) in dimension one, while the kernel we introduce in this work relies on (FG_p) . To avoid confusion, we will refer to (FG_p) (and (d_p)) as the Figalli–Gigli distance between persistence measures (in particular diagrams).

2.3 Kernel methods

Positive definite kernels. Given a set X and a symmetric function $k: X \times X \rightarrow \mathbb{R}$, k is said to be a positive semi-definite kernel if for every input $(x_1, \dots, x_n) \in X^n$ the matrix $(k(x_i, x_j))_{ij} \in \mathbb{R}^{n \times n}$ is itself positive semi-definite. Positive semi-definite kernels (simply referred to as kernels for the sake of concision) are useful as they are equivalent to feature maps: for every kernel k there exists a Hilbert space \mathcal{H} , called the Reproducing Kernel Hilbert Space (RKHS), and a feature map $\phi: X \rightarrow \mathcal{H}$ for which the following holds:

$$\forall x, y \in X, \quad \langle \phi(x), \phi(y) \rangle_{\mathcal{H}} = k(x, y). \quad (5)$$

As such, for all downstream learning tasks relying only on values of the inner product between elements of $\phi(X)$ (including many learning methods such as PCA, SVM, Ridge regression, etc.) only the value of $k(x, y)$ is necessary and no explicit knowledge of the embeddings $\phi(x), \phi(y)$ is required. This idea is known as the “kernel trick”.

Conditionally negative definite kernels. A common way of defining kernels is, given a Hilbert space with distance d , to set $k_{\sigma}(x, y) := \exp(-\frac{d(x, y)^2}{\sigma^2})$ for $\sigma > 0$. More generally, ([Berg et al. 1984](#), Theorem 3.2.2) states that setting $k_{\sigma}(x, y) := \exp(-\frac{f(x, y)}{\sigma^2})$

only yields a kernel if the function $f : X \times X \rightarrow \mathbb{R}$ is conditionally negative definite, that is:

$$\forall x_1, \dots, x_n \in X, \forall a_1, \dots, a_n \in \mathbb{R}, \quad \sum_{i=1}^n a_i = 0 \implies \sum_{i,j} a_i a_j f(x_i, x_j) \leq 0. \quad (6)$$

As shown in (Feragen et al. 2015), if the square of the distance function of a metric space (X, d) is conditionally negative definite, then X is flat (i.e. isometrically embeddable in a Hilbert space) or $\text{CAT}(0)$. However since \mathcal{D}^p is not $\text{CAT}(k)$ for any $k > 0$ (Turner et al. 2014), d_p^2 is not c.n.d for any p . This motivates the search for other ways to define kernels on PDs that would nonetheless be faithful to the geometry induced by the Figalli–Gigli distance.

2.4 Related works

2.4.1 The Sliced Wasserstein distance for probability measures

While the Wasserstein distance between probability measures (W_p) is expensive to compute (typically of order $O(N^3)$ for two measures supported on N points), the problem is known to become much simpler in dimension 1: in that case, the optimal transport plan γ is supported on the graph of the (unique) monotone map matching the quantiles of μ to that of ν , i.e. $x \mapsto F_\nu^{-1} \circ F_\mu(x)$, where $F_\rho(x) := \rho((-\infty, x])$ for a probability distribution ρ supported on \mathbb{R} . See (Santambrogio 2015, Ch. 2) for an extensive overview. In particular, if μ (resp. ν) is supported on N points $x_1 < \dots < x_N$ (resp. $y_1 < \dots < y_N$) with uniform weight $\frac{1}{N}$, one simply has $W_p(\mu, \nu)^p = \sum_{i=1}^n |x_i - y_i|^p$; reducing the computational cost to $O(N \log(N))$ (that of sorting the points).

Building on this idea, Rabin et al. (2011) introduce the *Sliced Wasserstein distance* between probability measures:

$$\text{SW}_p(\mu, \nu)^p := \int_{\theta \in S^{d-1}} W_p(\pi_\theta \# \mu, \pi_\theta \# \nu)^p d\theta, \quad (7)$$

where $\pi_\theta : \mathbb{R}^d \rightarrow \mathbb{R}$ is the projection $x \mapsto \langle x, \theta \rangle$, and $\#$ denotes the pushforward operator, i.e. $\pi_\theta \# \mu(A) = \mu(\pi_\theta^{-1}(A))$ for all Borel set $A \subset \mathbb{R}$. Approximating the integral by sampling K direction on the sphere S^{d-1} , one obtains a Wasserstein-like distance between probability measures that can be computed in $O(KN \log(N))$, a significant improvement over (W_p) .

The Sliced Wasserstein distance has attracted attention on the theoretical side (Nadjahi et al. 2020; Xi and Niles-Weed 2022; Park and Slepčev 2025) and has found several applications in machine learning (Deshpande et al. 2018; Nadjahi 2021). In particular Kolouri et al. (2016) observed that $(\mu, \nu) \mapsto \exp\left(-\frac{\text{SW}_2(\mu, \nu)^2}{2\sigma^2}\right)$ define a Gaussian-like kernel on the set of probability measures.

Several extensions have been proposed, for instance by replacing the average by a maximum in (7) (Deshpande et al. 2019; Kolouri et al. 2019; Boedihardjo 2025), and adapting it non-Euclidean geometries (Bonet et al. 2023a,b, 2025), where projections on lines are replaced by (Busemann) projection on geodesics. We will take inspiration

of this framework³ when defining the Sliced Figalli–Gigli distance between persistence diagrams.

2.4.2 Kernels for Persistence Diagrams

Several kernels on persistence diagrams have been proposed in the literature, typically divided in two classes. The first consists of defining kernels using explicit feature maps: given any map $\phi: \mathcal{D} \rightarrow \mathbb{R}^d$, one can build by definition a kernel by setting $(\mu, \nu) \mapsto \langle \phi(\mu), \phi(\nu) \rangle$. This includes for instance (Bubenik 2015; Adams et al. 2017). Closer to our purpose, the second class consists of defining implicit embeddings by directly building kernels on \mathcal{D} . For the sake of completeness, we briefly review the first two kernels of that type, before presenting in details the Sliced Wasserstein Kernel for persistence diagrams, from which our work is vastly inspired.

The persistence “Weighted Gaussian” (PWG) and “Scale-Space” (PSS) kernels. These two kernels are the first examples of PSD kernels on PDs defined through the kernel operator $k: \mathcal{D}^p(\Omega) \times \mathcal{D}^p(\Omega) \rightarrow \mathbb{R}$, instead of relying on an explicit embedding of PDs in a Hilbert space. The PWG kernel is introduced in (Kusano et al. 2016, 2018) and is defined in the following way. Let $C > 0$, μ be a persistence diagram, k_ρ be the gaussian kernel on $\Omega \times \Omega$ with parameter $\sigma > 0$ and \mathcal{H}_σ the corresponding RKHS. Define $\alpha_\mu := \sum_{x \in \tilde{spt}(\mu)} \arctan(Cd(x, \partial\Omega)^p)k_\sigma(\cdot, x) \in \mathcal{H}_\sigma$ to be the kernel mean embedding of μ weighted by the distance of its points to the diagonal. Eventually, define for $\tau > 0$

$$k_{\text{PWG}}(\mu_1, \mu_2) := \exp\left(-\frac{\|\alpha_{\mu_1} - \alpha_{\mu_2}\|^2}{\tau^2}\right). \quad (8)$$

The weighting of the embedding is motivated by the intuition that generators far from the diagonal carry more information than those that are close to it which typically reflect noise in the data.

The PSS kernel is defined in (Reininghaus et al. 2015) as the scalar product in $L^2(\Omega)$ of the two solutions of the heat diffusion equations with Dirac sources located at every point of the diagrams, namely:

$$k_{\text{PSS}}(\mu_1, \mu_2) := \frac{1}{8\pi\sigma} \sum_{\substack{p \in \tilde{spt}(\mu_1) \\ q \in \tilde{spt}(\mu_2)}} \exp\left(-\frac{\|p - q\|^2}{8\sigma}\right) - \exp\left(-\frac{\|p - \bar{q}\|^2}{8\sigma}\right), \quad (9)$$

where \bar{q} is the symmetric of q with respect to the diagonal, and $\sigma > 0$.

The Sliced Wasserstein Kernel (SWK). While PWG and PSS kernels can be proved to be stable, few is known about their discriminative power. To improve on this, Carrière et al. (2017) introduced a *Sliced Wasserstein kernel for persistence diagrams*, proposing an adaptation of the Sliced Wasserstein distance defined in (7) to the context of persistence diagrams.

³Though that literature focuses on negatively curved manifolds, which unfortunately does not cover our framework.

More precisely, given two persistence diagrams μ, ν and $\theta \in \mathbb{S}$, let $\mu_\theta := \pi_\theta \# (\mu + \pi_\Delta \# \nu)$ and $\nu_\theta := \pi_\theta \# (\nu + \pi_\Delta \# \mu)$ where π_θ is the orthogonal projection on the line l_θ going through $(0, 0)$ with angle θ to the diagonal and π_Δ is the orthogonal projection on the diagonal. This corresponds to projecting all the points of one diagram on the diagonal and then projecting those points along with the ones from the other diagram on l_θ . The kernel is then defined as:

$$k_{\text{SW}}(\mu, \nu) := \exp\left(-\frac{\text{SW}(\mu, \nu)}{\sigma^2}\right), \quad (10)$$

where $\text{SW}(\mu, \nu) = \int_{\mathbb{S}} W_1(\mu_\theta, \nu_\theta) d\theta$. This does yield a valid kernel since the Wasserstein distance on 1-dimensional measures is the L^1 distance between their quantile functions and is therefore c.n.d. This special form of the Wasserstein distance in one dimension also allows for efficient computation of this kernel as computing the quantile function of a 1-dimensional empirical measure boils down to sorting its points.

The authors also obtain bounds relating the SW distance and the usual d_1 distance for finite persistence diagrams. Namely,

$$\frac{d_1(\mu, \nu)}{1 + 2N(N - 1)} \leq \text{SW}(\mu, \nu) \leq 2\sqrt{2}d_1(\mu, \nu) \quad (11)$$

for any persistence diagrams $\mu, \nu \in \mathcal{D}(\Omega)$ with less than N points. This kernel proved to perform better in various tasks compared to the PSS and PWG kernels while also being more computationally efficient.

Remark 3 The SW distance is only defined for finite persistence diagrams and it is unclear whether the construction proposed in (Carrière et al. 2017) can be generalized to infinite persistence diagrams or persistence measures. In particular, projected measures μ_θ may not be Radon and as such the Wasserstein distance between them would be undefined. The formalism we introduce in this work, while substantially similar, presents the advantage of being faithfully defined for arbitrary persistence diagrams and measures. Furthermore, the bounds derived by Carrière et al. (2017) only consider the exponent $p = 1$, while the ones we present in this work hold for any $p \geq 1$.

3 The Sliced Figalli–Gigli distance and the induced kernel

Following the formalism introduced in (Divol and Lacombe 2020), we propose to adopt a similar approach as in (Carrière et al. 2017) by *slicing* the FG_p distance using *geodesics* emanating from the diagonal $\partial\Omega$.

3.1 Motivation & Definition

Consider $x, y \in \Omega$. Observe that as x and y approach $\partial\Omega$, one has $\text{FG}_p(\delta_x, \delta_y) \rightarrow 0$. Therefore, equipping $\mathcal{M}^p(\Omega)$ with the distance FG_p invites us to identify all points of

the diagonal $\partial\Omega$. More formally, FG_p induces a distance function Δ_p on $\overline{\Omega}$ defined by

$$\Delta_p^p(x, y) := \text{FG}_p^p(\delta_x, \delta_y) = \min(d(x, y)^p, d(x, \pi(x))^p + d(y, \pi(y))^p), \quad (12)$$

where π is the orthogonal projection on the diagonal. This distance is related to the natural distance induced by d on $\tilde{\Omega} := \Omega \cup \{\partial\Omega\}$ the quotient of the closed half-plane $\overline{\Omega}$ by $\partial\Omega$. Indeed, d induces a function \tilde{d} on $\tilde{\Omega}$ which satisfies $\tilde{d}(x, \partial\Omega) = d(x, \pi(x))$. We then define a distance ρ on $\tilde{\Omega}$ by setting:

$$\rho(x, y) = \min(\tilde{d}(x, y), \tilde{d}(x, \partial\Omega) + \tilde{d}(y, \partial\Omega)). \quad (13)$$

As such, $\tilde{\Omega}$ seems to better represent the geometry of the space of persistence diagrams endowed with FG_p . Following ideas introduced in (Bonet 2023), it would then seem natural to define a *Sliced Figalli–Gigli* metric by projecting on geodesics of $\tilde{\Omega}$ passing through a given origin O . Since the point $\partial\Omega$ plays a particular role in the structure of $\tilde{\Omega}$ we consider geodesics passing through this point. We have the following straightforward result.

Proposition 1 (Geodesics in $\tilde{\Omega}$) *Let $x, y \in \tilde{\Omega}$,*

1. *If $\rho(x, y) = \tilde{d}(x, y)$ the geodesic from x to y is the straight line from x to y , i.e.,*

$$\gamma_{x,y}(t) = (1 - t)x + ty. \quad (14)$$

2. *If $\rho(x, y) = \tilde{d}(x, \partial\Omega) + \tilde{d}(y, \partial\Omega) = \|x - \pi(x)\| + \|y - \pi(y)\|$, the geodesic from x to y goes through the diagonal and we have*

$$\gamma_{x,y}: \begin{cases} t \in [0, \alpha_x] \mapsto (1 - \frac{t}{\alpha_x})x + \frac{t}{\alpha_x}\partial\Omega \\ t \in [\alpha_x, 1] \mapsto (1 - \frac{t - \alpha_x}{\alpha_y})y + \frac{1-t}{\alpha_y}\partial\Omega \end{cases} \quad (15)$$

where $\alpha_x = \frac{\|x - \pi(x)\|}{\|x - \pi(x)\| + \|y - \pi(y)\|}$ and $\alpha_y = 1 - \alpha_x$.

As such, the geodesics originating from $\partial\Omega$ in $\tilde{\Omega}$ are of the form $G_t := \{(t, t) + s(-1, 1), s > 0\} \cup \{\partial\Omega\}$ (which we call the geodesic originating from $\partial\Omega$ with parameter t) for $t \in \mathbb{R}$. We then have the following result.

Proposition 2 (Projections on geodesics) *Let $t \in \mathbb{R}$. The projection on G_t is given by:*

$$\forall z \in \tilde{\Omega}, \quad \pi_t(z) = \begin{cases} (t, t) + \frac{z_2 - z_1}{2}(-1, 1) & \text{if } z_1 \leq t \leq z_2 \\ \partial\Omega & \text{otherwise.} \end{cases} \quad (16)$$

Proof Let $t \in \mathbb{R}$, G_t be the geodesic originating from $\partial\Omega$ with parameter t and \mathcal{G}_t its pullback in \mathbb{R}^2 i.e $\mathcal{G}_t := \{(t, t) + s(-1, 1), s \geq 0\}$. The projection of $z = (z_1, z_2) \in \Omega$ onto \mathcal{G}_t is then $\Pi_t(z) := (t, t) + \frac{z_2 - z_1}{2}(-1, 1)$. We then have

$$\|z - \Pi_t(z)\|^2 = 2 \left(\frac{z_1 + z_2}{2} - t \right)^2 \text{ and } \|z - \pi(z)\|^2 = \frac{(z_2 - z_1)^2}{2}. \quad (17)$$

Therefore,

$$\|z - \Pi_t(z)\|^2 = \|z - \pi(z)\|^2 \iff (z_1 - t)^2 + (z_2 - t)^2 = (z_2 - z_1)^2 \iff t = z_1 \text{ or } t = z_2. \quad (18)$$

The equation for π_t follows. \square

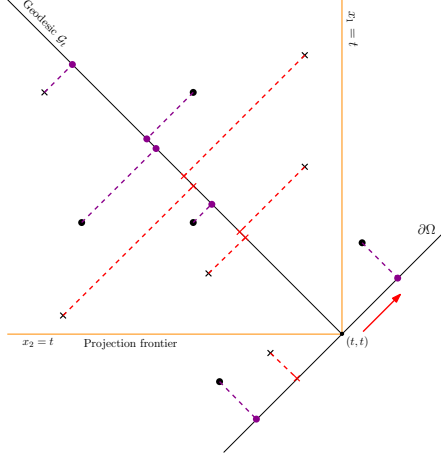


Fig. 1: Projections of two measures μ (circles) and ν (crosses) and their respective projections on the geodesic with parameter t . Points outside of the region delimited by $x_1 = t$ and $x_2 = t$ (which we denote Ω_t) are projected onto $\partial\Omega$. As t describes \mathbb{R} , Ω_t slides across the upper half-plane and captures information about different parts of the diagram. Observe also that a point x belongs to Ω_t for t belonging to an interval of length proportional to $d(x, \partial\Omega)$, hence the need for the renormalization we introduce.

The following lemma shows that the projection onto geodesics preserves the Radon structure of the measures.

Lemma 1 *Let $\mu \in \mathcal{M}(\Omega)$ and $t \in \mathbb{R}$. Then for any compact $A \subset G_t \setminus \{\partial\Omega\}$, $\pi_t \# \mu(A) < +\infty$.*

Proof Let $M := \sup(\{d(x, \partial\Omega), x \in A\})$. Observe that since $A \subset G_t \setminus \partial\Omega$, we have $\pi_t^{-1}(A) \subset C := \{z \in \Omega, t - \sqrt{2}M \leq z_1 \leq t \text{ and } t \leq z_2 \leq t + \sqrt{2}M\}$ which is a compact subset of Ω . Hence, $\pi_t \# \mu(A) = \mu(\pi_t^{-1}(A)) < +\infty$. \square

Remark 4 The above Lemma shows that the pushforward of any Radon measure $\mu \in \mathcal{M}(\Omega)$ by the projection π_t is still a Radon measure when restricting it to $\mathcal{G}_t \setminus \partial\Omega$. The fact that it

is not a Radon measure on \mathcal{G}_t (since the point $\partial\Omega$ may have infinite mass) won't come into question as we will only consider the restriction of the pushforward measure to $\mathcal{G}_t \setminus \partial\Omega$ later on (which we still denote by $\pi_t \# \mu$).

One may then want to consider the quantity $(\int_{t \in \mathbb{R}} \text{FG}_p^p(\pi_t \# \mu, \pi_t \# \nu) dt)^{\frac{1}{p}}$ to define a distance on $\mathcal{M}^p(\Omega)$. However, given $\mu \in \mathcal{M}(\Omega)$, we have

$$\int_{t \in \mathbb{R}} \text{FG}_p^p(\pi_t \# \mu, \emptyset) dt = \int_{t \in \mathbb{R}} \left(\int_{\Omega} d(\pi_t(z), \partial\Omega)^p d\mu(z) \right) dt \quad (19)$$

$$= \int_{\Omega} (z_2 - z_1) d(z, \partial\Omega)^p d\mu(z) \quad (20)$$

$$= \sqrt{2} \text{Pers}_{p+1}(\mu), \quad (21)$$

and therefore the above quantity is only well-defined on $\mathcal{M}^{p+1}(\Omega)$ and not on $\mathcal{M}^p(\Omega)$. To circumvent this, we introduce the following renormalization. Given $\mu \in \mathcal{M}^p(\Omega)$ define $\tilde{\mu}$ by setting for any Borel set A

$$\tilde{\mu}(A) := \int_A \frac{d\mu(x)}{d(x, \partial\Omega)}. \quad (22)$$

This way, $\tilde{\mu} \in \mathcal{M}^{p+1}(\Omega)$ since $\tilde{\mu}(A) < +\infty$ for all compact sets of Ω (every compact of the open half-plane Ω is at a positive distance from $\partial\Omega$) and $\text{Pers}_{p+1}(\tilde{\mu}) = \text{Pers}_p(\mu) < +\infty$. This yields the following definition.

Definition 1 (The Sliced Figalli–Gigli distance) Let $p \geq 1$ and $\mu, \nu \in \mathcal{M}^p(\Omega)$ and $\tilde{\mu}, \tilde{\nu}$ their normalization following (22). The Sliced Figalli–Gigli (SFG) distance between μ and ν is defined as

$$\text{SFG}_p(\mu, \nu) := \frac{1}{\sqrt{2}} \left(\int_{\mathbb{R}} \text{FG}_p^p(\pi_t \# \tilde{\mu}, \pi_t \# \tilde{\nu}) dt \right)^{\frac{1}{p}}. \quad (\text{SFG}_p)$$

Note that given $\mu \in \mathcal{M}^p(\Omega)$ we have

$$\text{SFG}_p^p(\mu, \emptyset) = \frac{1}{\sqrt{2}} \int_{t \in \mathbb{R}} \left(\int_{\Omega} d(\pi_t(z), \partial\Omega)^p \frac{d\mu(z)}{d(z, \partial\Omega)} \right) dt \quad (23)$$

$$= \frac{1}{\sqrt{2}} \int_{\Omega} (z_2 - z_1) d(z, \partial\Omega)^{p-1} d\mu(z) \quad (24)$$

$$= \text{Pers}_p(\mu), \quad (25)$$

and therefore by Hölder's inequality,

$$\text{SFG}_p(\mu, \nu) \leq \frac{1}{\sqrt{2}} \left(\int_{t \in \mathbb{R}} (\text{FG}_p(\pi_t \# \mu, \emptyset) + \text{FG}_p(\pi_t \# \nu, \emptyset))^p dt \right)^{\frac{1}{p}} \quad (26)$$

$$\leq \text{SFG}_p(\mu, \emptyset) + \text{SFG}_p(\nu, \emptyset) < +\infty, \quad (27)$$

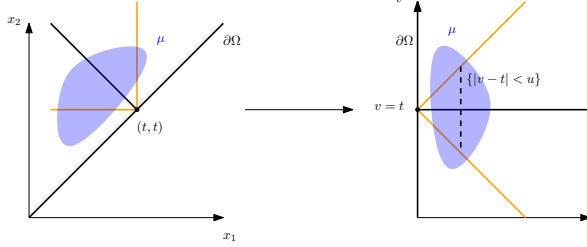


Fig. 2: Change of coordinates used in the proof of Lemma 2.

ensuring that (SFG_p) is well defined for persistence diagrams and measures in $\mathcal{M}^p(\Omega)$.

Equation (23) immediately gives the following proposition.

Proposition 3 *Let $\mu \in \mathcal{M}^p(\Omega)$, and \emptyset denote the empty diagram. One has*

$$\text{SFG}_p(\mu, \emptyset) = \text{FG}_p(\mu, \emptyset) = \text{Pers}_p(\mu). \quad (28)$$

Eventually, we have the following central proposition.

Proposition 4 *SFG_p is a distance on $\mathcal{M}^p(\Omega)$.*

Proof The fact that FG_p is a distance immediately implies that SFG_p is non-negative and satisfies the triangle inequality. Eventually, let $\mu, \nu \in \mathcal{M}^p(\Omega)$ such that $\text{SFG}_p(\mu, \nu) = 0$. This implies that their projections (after normalization) on $\mathcal{G}_t \setminus \{\partial\Omega\}$ coincide for almost every $t \in \mathbb{R}$. The injectivity of that transform is proved in the following lemma, yielding $\mu = \nu$. \square

Lemma 2 *Let $\mu, \nu \in \mathcal{M}^p(\Omega)$ and let $(\tilde{\mu}_t)_{t \in \mathbb{R}}, (\tilde{\nu}_t)_{t \in \mathbb{R}}$ be their respective transform by the map $\mu \mapsto \pi_t \# \mu \upharpoonright_{\mathcal{G}_t \setminus \{\partial\Omega\}}$. Assume that t -a.e. (with respect to the Lebesgue measure on \mathbb{R}), one has $\tilde{\mu}_t = \tilde{\nu}_t$. Then $\mu = \nu$.*

Proof To alleviate notation in this proof, we consider the change of coordinates $(x_1, x_2) \mapsto \left(\frac{y-x}{2}, \frac{x+y}{2}\right) =: (u, v)$, and keep the same notation ($\mu, \tilde{\mu}_t, \Omega, \partial\Omega$, etc.) with this new coordinate system, see Fig. 2 for an illustration.

Let $\varphi \in \mathcal{C}_c^\infty((0, +\infty))$ be a smooth, compactly supported, test function. One has

$$\langle \varphi, \tilde{\mu}_t \rangle = \int_{(u, v) \in \Omega} \varphi(u) \mathbf{1}_{(v-u, v+u)}(t) d\mu(u, v), \quad (29)$$

where $\mathbf{1}_{(v-u, v+u)}$ is the indicator function of the set $\{|v - t| < u\}$. The first order derivative of that function with respect to t in a distributional sense is $t \mapsto \int \varphi(u) [\delta_{v-u}(t) - \delta_{v+u}(t)] d\mu$. Therefore, considering another test function $\psi \in \mathcal{C}_c^\infty(\mathbb{R})$, one has

$$\int \psi'(t) \langle \varphi, \tilde{\mu}_t \rangle dt = \int \varphi(u) [\psi(v-u) - \psi(v+u)] d\mu(u, v). \quad (30)$$

Therefore, the equality for almost every $t \in \mathbb{R}$ between $\tilde{\mu}_t$ and $\tilde{\nu}_t$ implies that for any $\varphi, \psi \in \mathcal{C}_c^\infty((0, +\infty)) \times \mathcal{C}_c^\infty(\mathbb{R})$, one has

$$\int \varphi(u)[\psi(v-u) - \psi(v+u)] \, d(\mu - \nu)(u, v) = 0. \quad (31)$$

Let $\eta := \mu - \nu$, let π be the first marginal of $|\eta|(u, v)$ and consider the disintegration $d\eta = d\eta_u \otimes d\pi(u)$. Note that the condition $\mu, \nu \in \mathcal{M}^p(\Omega)$ imposes that η_u has finite total mass on \mathbb{R} for π -a.e. $u > 0$. From (31), denoting τ_u the translation $w \mapsto w + u$, we have for all test function $\varphi, \psi \in \mathcal{C}_c^\infty((0, +\infty)) \times \mathcal{C}_c^\infty(\mathbb{R})$,

$$\int_{u>0} \varphi(u) \left[\int \psi(w) d\tau_{-u} \# \eta_u(w) - \int \psi(w) d\tau_u \# \eta_u(w) \right] d\pi(u) = 0. \quad (32)$$

Therefore, we deduce that for π -a.e. $u > 0$, one has $\int \psi(w) d[\tau_{-u} \# \eta_u - \tau_u \# \eta_u](w) = 0$ for all test function ψ , and thus that $\eta_u = \tau_{2u} \eta_u$. Eventually, η_u being of finite total mass, this translation invariance imposes $\eta_u = 0$ for π -a.e. $u > 0$, thus $\eta = 0$, that is $\mu = \nu$. \square

Remark 5 (On the choice of the projection) The projection on the geodesic \mathcal{G}_t has no need to be the orthogonal projection. In particular, one may choose another map $z \mapsto \tilde{\pi}_t(z)$ that has nicer properties than the one defined above. For this reason, we study in Appendix A a *continuous projection* which, contrary to the orthogonal projection, is Lipschitz continuous. One may hope that this increased regularity would lead to better theoretical guarantees, but our study did not showcase any significant improvement of this alternative projection over the naive one we present here. We still include this discussion in the appendix for the sake of completeness.

3.2 The Sliced Figalli–Gigli kernel

In this section, we define the kernel associated to the SFG_p distance. As mentioned in Section 2.3, we first need to prove that the SFG_p distance is c.n.d. which, similarly to what is done in (Carrière et al. 2017), will be a consequence of the special form of the FG_p distance in one dimension.

3.2.1 The FG_p problem in 1D

The main result of this subsection, Proposition 7, is to show that in dimension one, for Radon measures supported on the open half-line $\mathbb{R}_{>0} = (0, +\infty)$, the Figalli–Gigli distance admits a simple closed form which, as its Wasserstein counterpart (W_p), boils down to considering monotone matchings (i.e. sorting the point for discrete measures). The subtlety is to properly account for the role played by the diagonal $\partial\Omega$ and the fact that, in contrast to probability measures, persistence measures and diagram may have infinite total mass, preventing us from straightforwardly use quantile functions to define monotone matching.

Let $\mu, \nu \in \mathcal{M}^p(\mathbb{R}_{>0})$, we want to characterize γ_p the optimal transport plan reaching the infimum in FG_p (so here $\Omega = \mathbb{R}_{>0}$ et $\partial\Omega = \{0\}$).

Lemma 3 *Suppose $p > 1$, for all $(x_1, y_1), (x_2, y_2) \in \text{spt}(\gamma_p)$, if $x_1 < x_2$ then $y_1 \leq y_2$.*

Proof From (Figalli and Gigli 2010, Prop. 2.3), $\text{spt}(\gamma_p)$ is Δ_p^p -cyclically monotone, and therefore, for all $(x_1, y_1), (x_2, y_2) \in \text{spt}(\gamma_p)$ we have

$$|x_1 - y_1|^p + |x_2 - y_2|^p \leq |x_1 - y_2|^p + |x_2 - y_1|^p. \quad (33)$$

Assume that $x_1 < x_2$, then if $y_1 > y_2$ one has that $y_1 - x_1 > y_1 - x_2 > y_2 - x_2$ and $y_1 - x_1 > y_2 - x_1 > y_2 - x_2$. By strict convexity of $x \mapsto x^p$ for $p > 1$, the following then holds:

$$\frac{|y_1 - x_2|^p - |y_2 - x_2|^p}{y_1 - y_2} < \frac{|y_1 - x_1|^p - |y_2 - x_2|^p}{(y_1 - x_1) - (y_2 - x_2)} < \frac{|y_1 - x_1|^p - |y_1 - x_2|^p}{x_2 - x_1} \quad (34)$$

$$\frac{|y_2 - x_1|^p - |y_2 - x_2|^p}{x_2 - x_1} < \frac{|y_1 - x_1|^p - |y_2 - x_2|^p}{(y_1 - x_1) - (y_2 - x_2)} < \frac{|y_1 - x_1|^p - |y_2 - x_1|^p}{y_2 - y_1} \quad (35)$$

From there we get that $|y_2 - x_1|^p + |y_1 - x_2|^p < |y_1 - x_1|^p + |y_2 - x_2|^p$ which is absurd. As such, $y_1 \leq y_2$. \square

We will now prove, similarly to how it is done in the case of traditional Optimal Transport (Santambrogio 2015), that FG_p in dimension 1 is actually an L^p distance.

Definition 2 Let $\mu \in \mathcal{M}(\mathbb{R}_+)$, for $x \in \mathbb{R}_+$ we define:

$$F_\mu(x) = \mu([x, +\infty)) \text{ and } F_\mu^{-1}(x) = \sup(\{t \in \mathbb{R}_+ : F_\mu(t) \geq x\}), \quad (36)$$

agreeing that $F_\mu^{-1}(x) = 0$ if $\{t \in \mathbb{R}_+ : F_\mu(t) \geq x\} = \emptyset$.

Remark 6 These definitions are very close to the standard definitions for the distribution function of a measure and its pseudo-inverse. The main difference with our constructions (which we will refer to with the same names) is the "direction" of the quantiles: we define them as $\mu([x, +\infty))$ instead of the standard $\mu((-\infty, x])$. The latter could be ill-defined if μ has infinite total mass close to $\partial\Omega$, making the alternate definition necessary.

Remark 7 F_μ characterises μ since the family $\{[x, +\infty), x \in \mathbb{R}_+\}$ generates all the Borel sets of \mathbb{R}_+ . Furthermore, the following holds:

$$F_\mu^{-1}(x) \geq a \iff F_\mu(a) \geq x. \quad (37)$$

Proposition 5 Let $\mu, \nu \in \mathcal{M}(\mathbb{R}_+)$. One has

$$F_\mu^{-1} \# \mathcal{L}^1([0, +\infty)) = \mu. \quad (38)$$

Furthermore, denote $\gamma_{mon} = (F_\mu^{-1}, F_\nu^{-1}) \# \mathcal{L}^1([0, +\infty))$, then $\gamma_{mon} \in \text{Adm}(\mu, \nu)$ and $\gamma_{mon}([a, +\infty) \times [b, +\infty)) = \min(F_\mu(a), F_\nu(b))$.

Proof We have

$$F_{F_\mu^{-1} \# \mathcal{L}^1([0, +\infty))}(x) = \mathcal{L}^1(\{x \geq 0, F_\mu^{-1}(x) \geq a\}) \quad (39)$$

$$= \mathcal{L}^1(\{x \geq 0 : F_\mu(a) \geq x\}) \quad (\text{see 37}) \\ = F_\mu(a). \quad (40)$$

As such, these two measures have the same distribution function so $F_\mu^{-1} \# \mathcal{L}^1([0, +\infty)) = \mu$. Then:

$$\iint_{A \times \mathbb{R}_+} d\gamma_{mon}(x, y) = \int_{\mathbb{R}_+} 1_A(F_\mu^{-1}(x)) 1_{\mathbb{R}_+} F_\nu^{-1}(x) dx \quad (41)$$

$$= \int_A d(F_\mu^{-1} \# dx)(x) \quad (42)$$

$$= \mu(A). \quad (\text{according to the first part})$$

Similarly, one can show that the second marginal of γ_{mon} is ν , so $\gamma_{mon} \in \text{Adm}(\mu, \nu)$. Then,

$$\gamma_{mon}([a, +\infty), [b, +\infty)) = \mathcal{L}^1(\{x \geq 0 : F_\mu^{-1}(x) \geq a, F_\nu^{-1}(x) \geq b\}) \quad (43)$$

$$= \mathcal{L}^1(\{x \geq 0 : F_\mu(a) \geq x, F_\nu(b) \geq x\}) \quad (44)$$

$$= \min(F_\mu(a), F_\nu(b)). \quad (45)$$

which is the desired equality. \square

Proposition 6 γ_{mon} is optimal.

Proof We still suppose that $p > 1$. Let γ_p denote the optimal transport plan, then from 3 we get that for all $(x, y), (x', y') \in \text{spt}(\gamma_p)$, $x < x' \implies y \leq y'$. Consider $a, b \in \mathbb{R}_+$ and let $A = [a, +\infty) \times [0, b)$ and $B = [0, a) \times [b, +\infty)$. If $\gamma_p(A) > 0$ and $\gamma_p(B) > 0$, then we can find $(x, y) \in A \cap \text{spt}(\gamma_p)$ and $(x', y') \in B \cap \text{spt}(\gamma_p)$. But then we would have $x' < x$ and $y' > y$ which is absurd.

Hence,

$$\gamma([a, +\infty) \times [b, +\infty)) = \min(\gamma([a, +\infty) \times [b, +\infty) \cup A), \gamma([a, +\infty) \times [b, +\infty) \cup B)). \quad (46)$$

However, $\gamma([a, +\infty) \times [b, +\infty) \cup A) = \gamma([a, +\infty) \times \mathbb{R}_+) = F_\mu(a)$ and $\gamma([a, +\infty) \times [b, +\infty) \cup B) = \gamma(\mathbb{R}_+ \times [b, +\infty)) = F_\nu(b)$. Therefore, γ_p and γ_{mon} coincide on sets of the form $[a, +\infty) \times [b, +\infty)$ which is enough to conclude that $\gamma_p = \gamma_{mon}$.

The case for $p = 1$ is handled with the same limit argument as in (Santambrogio 2015). Lemma 2.10 in (Santambrogio 2015) states that for every $\varepsilon > 0$ there exist a strictly convex function c_ε such that $|\cdot| \leq c_\varepsilon \leq \varepsilon + (1 + \varepsilon)|\cdot|$. We then get, given $\gamma \in \text{Adm}(\mu, \nu)$:

$$\int_{\mathbb{R}_+} |x - y| d\gamma_{mon}(x, y) \leq \int_{\mathbb{R}_+} c_\varepsilon(x - y) d\gamma_{mon}(x, y) \quad (47)$$

$$\leq \int_{\mathbb{R}_+} c_\varepsilon(x - y) d\gamma(x, y) \quad (\gamma_{mon} \text{ is optimal since } c_\varepsilon \text{ is strictly convex})$$

$$\leq \varepsilon + \int_{\mathbb{R}_+} (1 + \varepsilon)|x - y| d\gamma(x, y). \quad (48)$$

Taking the limit as $\varepsilon \rightarrow 0$ then yields the desired result. \square

From this we deduce the following result.

Proposition 7 Let $\mu, \nu \in \mathcal{M}^p(\mathbb{R}_{>0})$,

$$\text{FG}_p^p(\mu, \nu) = \int_{\mathbb{R}_{>0}} |F_\mu^{-1}(t) - F_\nu^{-1}(t)|^p dt. \quad (49)$$

This is analogous to the special form of the standard Wasserstein distance in 1D.

3.2.2 The SFG kernel

Before defining the SFG kernel we first need to prove that SFG is CND.

Proposition 8 *For all $1 \leq p \leq 2$, SFG_p^p is CND.*

Proof Let $1 \leq p \leq 2$, $\mu_1, \dots, \mu_n \in \mathcal{M}^p(\Omega)$ and $a_1, \dots, a_n \in \mathbb{R}$ such that $\sum_i a_i = 0$. We have

$$\sum_{i,j} a_i a_j \text{SFG}_p^p(\mu_i, \mu_j) = \frac{1}{\sqrt{2}^p} \sum_{i,j} a_i a_j \int_{\mathbb{R}} \text{FG}_p^p(\pi_t \# \tilde{\mu}_i, \pi_t \# \tilde{\mu}_j) dt \quad (50)$$

$$= \frac{1}{\sqrt{2}^p} \sum_{i,j} a_i a_j \int_{\mathbb{R}} \int_{\mathbb{R}_+} |F_{\pi_t \# \tilde{\mu}_i}^{-1}(s) - F_{\pi_t \# \tilde{\mu}_j}^{-1}(s)|^p ds dt \quad (51)$$

$$= \frac{1}{\sqrt{2}^p} \int_{\mathbb{R}} \int_{\mathbb{R}_+} \left(\sum_{i,j} a_i a_j |F_{\pi_t \# \tilde{\mu}_i}^{-1}(s) - F_{\pi_t \# \tilde{\mu}_j}^{-1}(s)|^p \right) ds dt. \quad (52)$$

We denote by d the euclidean distance on \mathbb{R} . Since d^2 is CND, Theorem 4.7 in (Wells and Williams 1975) states that d^p also is. As such,

$$\forall t \in \mathbb{R}, \quad \sum_{i,j} a_i a_j |F_{\pi_t \# \tilde{\mu}_i}^{-1}(s) - F_{\pi_t \# \tilde{\mu}_j}^{-1}(s)|^p \leq 0. \quad (53)$$

Thus we obtain $\sum_{i,j} a_i a_j \text{SFG}_p(\mu_i, \mu_j) \leq 0$ i.e. SFG_p^p is CND. \square

Hence, (Berg et al. 1984, Theorem 3.2.2) allows us to define a valid kernel on $\mathcal{M}^p(\Omega)$ through

$$k_{\text{SFG}_p}(\mu, \nu) := \exp \left(- \frac{\text{SFG}_p^p(\mu, \nu)}{\sigma^2} \right). \quad (54)$$

Note that this kernel is defined for $p \in [1, 2]$; for $p = 1$ one has a Laplace-like kernel on persistence measures while for $p = 2$ this kernel resembles a Gaussian kernel.

3.3 Stability and equivalence of topologies

In this subsection, we prove the stability of the SFG_p distance with respect to the FG_p distance as well as the equivalence of the topologies induced by these norms.

3.3.1 Stability

We want to prove that the SFG_p distance is stable with respect to the FG_p distance, i.e. obtain an inequality of the form $\text{SFG}_p(\mu, \nu) \leq C_p \text{FG}_p(\mu, \nu)$ for some constant C_p . We prove the following result.

Theorem 1 *Let $\mu, \nu \in \mathcal{M}^p(\Omega) \cap \mathcal{M}^\infty(\Omega)$, one has:*

$$\text{SFG}_p^p(\mu, \nu) \leq \text{FG}_p^p(\mu, \nu) + 2M^{p-1} \iint_{\Omega \times \Omega} d(x, y) d\gamma(x, y), \quad (55)$$

where $M := \max(\text{Pers}_\infty(\mu), \text{Pers}_\infty(\nu))$. For $p = 1$, the result simplifies to

$$\forall \mu, \nu \in \mathcal{M}^1(\Omega), \quad \text{SFG}_1(\mu, \nu) \leq 3\text{FG}_1(\mu, \nu), \quad (56)$$

in particular one does not need to assume that $\max(\text{Pers}_\infty(\mu), \text{Pers}_\infty(\nu)) < \infty$.

Establishing the stability of the Sliced Wasserstein distance with respect to the Wasserstein distance derived in (Carrière et al. 2017) when $p = 1$ (see (11)) relies on the idea that one may obtain a transport plan between the projection of two measures μ, ν from the transport plan γ between the original measures by simply considering the pushforward of γ by the projection. Our proof relies on the same idea though the construction of an admissible transport plan between the projected measures is more technical as we are renormalizing our measures before projecting them on geodesics.

Let $\mu, \nu \in \mathcal{M}^p(\Omega)$ and $\gamma \in \text{Adm}(\mu, \nu)$, we can construct an element $\tilde{\gamma}$ of $\text{Adm}(\tilde{\mu}, \tilde{\nu})$ from γ by setting for $A, B \subset \Omega$:

$$\tilde{\gamma}(A \times B) := \iint_{A \times B} \frac{1}{\max(d(x, \partial\Omega), d(y, \partial\Omega))} d\gamma(x, y). \quad (57)$$

Furthermore, let $A_+ = \{(x, y) \in A \times \Omega : d(y, \partial\Omega) \geq d(x, \partial\Omega)\}$ and $B_+ = \{(x, y) \in \Omega \times B : d(x, \partial\Omega) \geq d(y, \partial\Omega)\}$ and define:

$$\tilde{\gamma}(A \times \partial\Omega) := \iint_{A \times \partial\Omega} \frac{1}{d(x, \partial\Omega)} d\gamma(x, y) + \iint_{A_+} \left(\frac{1}{d(x, \partial\Omega)} - \frac{1}{d(y, \partial\Omega)} \right) d\gamma(x, y) \quad (58)$$

$$\tilde{\gamma}(\partial\Omega \times B) := \iint_{\partial\Omega \times B} \frac{1}{d(y, \partial\Omega)} d\gamma(x, y) + \iint_{B_+} \left(\frac{1}{d(y, \partial\Omega)} - \frac{1}{d(x, \partial\Omega)} \right) d\gamma(x, y). \quad (59)$$

Proposition 9 *With the above definition, $\tilde{\gamma} \in \text{Adm}(\tilde{\mu}, \tilde{\nu})$.*

Proof We have

$$\tilde{\gamma}(\overline{\Omega} \times B) = \iint_{\partial\Omega \times B} d\tilde{\gamma}(x, y) + \iint_{B_+} d\tilde{\gamma}(x, y) + \iint_{B_-} d\tilde{\gamma}(x, y) \quad (60)$$

$$= \iint_{\partial\Omega \times B} \frac{d\gamma(x, y)}{d(y, \partial\Omega)} + \iint_{B_+} \left(\frac{1}{d(y, \partial\Omega)} - \frac{1}{d(x, \partial\Omega)} \right) d\gamma(x, y) \quad (61)$$

$$+ \iint_{B_+} \frac{1}{d(x, \partial\Omega)} d\gamma(x, y) + \iint_{B_-} \frac{1}{d(y, \partial\Omega)} d\gamma(x, y) \quad (62)$$

$$= \iint_{\overline{\Omega} \times B} \frac{1}{d(y, \partial\Omega)} d\gamma(x, y) = \tilde{\nu}(B). \quad (63)$$

Similarly, we have $\tilde{\gamma}(A \times \overline{\Omega}) = \tilde{\mu}(A)$.

We now just need to verify that $\tilde{\gamma}$ takes finite values on compacts of $\Omega \times \Omega \setminus \partial\Omega \times \partial\Omega$ (cf. (Figalli and Gigli 2010)), transport plans are Radon measures on that space). Consider then C a compact of that space. Observe that, since $\partial\Omega \times \partial\Omega$ is closed, $\varepsilon := d(C, \partial\Omega \times \partial\Omega) > 0$. We can then write $C \subset \bigcup_{(x, y) \in C} B(x, \frac{\varepsilon}{4}) \times B(y, \frac{\varepsilon}{4})$ from which we extract a finite subcover to get $C \subset \bigcup_{i=1}^n \overline{B(x_i, \frac{\varepsilon}{4}) \times B(y_i, \frac{\varepsilon}{4})}$. Therefore, it suffices to show that $\gamma(A \times B)$ is finite for all $A \times B$ compact de $\Omega \times \Omega$ such that $d(A \times B, \partial\Omega \times \partial\Omega) > 0$.

Let A, B be such compacts. Since $d(A \times B, \partial\Omega \times \partial\Omega) > 0$, necessarily $d(A, \partial\Omega) > 0$ or $d(B, \partial\Omega) > 0$. Suppose it is the case for A . We then write $A \times B \subset A \times (B \setminus \partial\Omega) \cup A \times \partial\Omega$ from which we get $\tilde{\gamma}(A \times B) \leq \tilde{\gamma}(A \times B \setminus \partial\Omega) + \tilde{\gamma}(A \times \partial\Omega)$. Furthermore,

$$\tilde{\gamma}(A \times (B \setminus \partial\Omega)) = \iint_{A \times B \setminus \partial\Omega} \frac{1}{\max(d(x, \partial\Omega), d(y, \partial\Omega))} d\gamma(x, y) \quad (64)$$

$$\leq \frac{1}{d(A, \partial\Omega)} \iint_{A \times \overline{\Omega}} d\gamma(x, y) = \frac{\mu(A)}{d(A, \partial\Omega)} < +\infty, \quad (65)$$

and

$$\tilde{\gamma}(A \times \partial\Omega) = \iint_{A \times \partial\Omega} \frac{d\gamma(x, y)}{d(x, \partial\Omega)} + \iint_{A_+} \left(\frac{1}{d(x, \partial\Omega)} - \frac{1}{d(y, \partial\Omega)} \right) d\gamma(x, y) \quad (66)$$

$$\leq \frac{1}{d(A, \partial\Omega)} \iint_{A \times \overline{\Omega}} d\gamma(x, y) \quad (67)$$

$$= \frac{\mu(A)}{d(A, \partial\Omega)} < +\infty, \quad (68)$$

which concludes the proof. \square

We also have the following straightforward lemma.

Lemma 4 *Let $x = (x_1, x_2)$ and $y = (y_1, y_2) \in \Omega$. We have*

$$\int_{\mathbb{R}} d(\pi_t(x), \pi_t(y))^p dt \leq \sqrt{2} \max(d(x, \partial\Omega), d(y, \partial\Omega)) \|x - y\|^p \quad (69)$$

$$+ \sqrt{2} \max(d(x, \partial\Omega), d(y, \partial\Omega))^p \|x - y\|. \quad (70)$$

Proof Assume $x_1 \leq y_1 \leq x_2 \leq y_2$. Then for all $t \notin [x_1, y_2]$, $d(\pi_t(x), \pi_t(y)) = 0$ and we have

$$\int_{x_1}^{y_1} d(\pi_t(x), \pi_t(y))^p dt = d(x, \partial\Omega)^p (y_1 - x_1) \text{ and } \int_{x_2}^{y_2} d(\pi_t(x), \pi_t(y))^p dt = d(y, \partial\Omega)^p (y_2 - x_2). \quad (71)$$

Furthermore, since for all $x_2 \leq t \leq y_1$, $d(\pi_t(x), \pi_t(y)) \leq \|x - y\|$, we also have

$$\int_{y_1}^{x_2} d(\pi_t(x), \pi_t(y))^p dt \leq (x_2 - y_1) \|x - y\|^p \leq \max(d(x, \partial\Omega), d(y, \partial\Omega)) \|x - y\|^p. \quad (72)$$

Combining these inequalities yields the desired result. The calculation is the same when $x_1 \leq y_1 \leq y_2 \leq x_2$. \square

We can now prove Theorem 1.

Proof Let $\mu, \nu \in \mathcal{M}^p(\Omega) \cap \mathcal{M}^\infty(\Omega)$. Observe that $\text{spt}(\gamma) \cap \{(x, y) \in \Omega^2 : x_1 \leq x_2 \leq y_1 \leq y_2 \text{ or } y_1 \leq y_2 \leq x_1 \leq x_2\} = \emptyset$. Hence, using 4, we get

$$\int_{\mathbb{R}} \iint_{\Omega \times \Omega} d(\pi_t(x), \pi_t(y))^p d\tilde{\gamma}(x, y) dt \leq \sqrt{2} \iint_{\Omega \times \Omega} \|x - y\|^p d\gamma(x, y) \quad (73)$$

$$+ \sqrt{2} \iint_{\Omega \times \Omega} \max(d(x, \partial\Omega), d(y, \partial\Omega))^{p-1} \|x - y\| d\gamma(x, y). \quad (74)$$

Then, one has

$$\int_{\mathbb{R}} \iint_{\Omega \times \partial\Omega} d(\pi_t(x), \pi_t(y))^p d\tilde{\gamma}(x, y) dt \leq \sqrt{2} \iint_{\Omega \times \partial\Omega} d(x, \partial\Omega)^p d\gamma(x, y) \quad (75)$$

$$+ \sqrt{2} \iint_{\Omega_{1,+}} d(x, \partial\Omega)^{p+1} \left(\frac{1}{d(x, \partial\Omega)} - \frac{1}{d(y, \partial\Omega)} \right) d\gamma(x, y), \quad (76)$$

where $\Omega_{1,+} = \{(x, y) \in \Omega \times \Omega : d(y, \partial\Omega) \geq d(x, \partial\Omega)\}$ and $\Omega_{2,+} = \{(x, y) \in \Omega \times \Omega : d(x, \partial\Omega) \geq d(y, \partial\Omega)\}$. We also have a similar inequality when integrating over $\partial\Omega \times \Omega$. Combining those results, we get

$$\begin{aligned} \sqrt{2} \text{SFG}_p^p(\mu, \nu) &\leq \sqrt{2} \text{FG}_p^p(\mu, \nu) \\ &+ \sqrt{2} \iint_{\Omega \times \Omega} \max(d(x, \partial\Omega), d(y, \partial\Omega))^{p-1} d(x, y) d\gamma(x, y) \\ &+ \sqrt{2} \iint_{\Omega \times \Omega} \frac{\min(d(x, \partial\Omega), d(y, \partial\Omega))^p}{\max(d(x, \partial\Omega), d(y, \partial\Omega))} d(x, y) d\gamma(x, y), \end{aligned} \quad (77)$$

from which we deduce the result of Theorem 1. \square

It is unfortunately impossible to get a uniform upper bound (that is a bound given by a constant factor of the FG_p distance) when $p > 1$. Indeed, consider $\mu_n = \delta_{(-n, n)}$ and $\nu_n = \delta_{(-n - \frac{1}{\ln(n)}, n + \frac{1}{\ln(n)})}$ on one hand we get $\text{FG}_p(\mu_n, \nu_n) = \frac{\sqrt{2}}{\ln(n)}$ and on the other we have

$$\text{SFG}_p^p(\mu_n, \nu_n) \geq \sqrt{2}^{p+1} n^{p+1} \left(\frac{1}{\sqrt{2}n} - \frac{1}{\sqrt{2}(n + \frac{1}{\ln(n)})} \right) \underset{n \rightarrow +\infty}{\sim} C \frac{n^{p-1}}{\ln(n)}. \quad (78)$$

In particular, $\text{FG}_p(\mu_n, \nu_n) \xrightarrow{n \rightarrow +\infty} 0$ and $\text{SFG}_p(\mu_n, \nu_n) \xrightarrow{n \rightarrow +\infty} +\infty$.

Similarly, it is not possible to get a uniform lower bound of the form $C_p \text{SFG}_p \leq \text{FG}_p$. Indeed, by considering the following two diagrams $\mu_n = \{(k \frac{\sqrt{2}}{n}, (k+1) \frac{\sqrt{2}}{n}), k \in [0, \lceil n^p \rceil]\}$ and $\nu_n = \{(k + \frac{1}{2}) \frac{\sqrt{2}}{n}, (k+1 + \frac{1}{2}) \frac{\sqrt{2}}{n}, k \in [0, \lceil n^p \rceil]\}$. We then have $\text{SFG}_p^p(\mu_n, \nu_n) = \frac{1}{n^p}$ and $\text{FG}_p(\mu_n, \nu_n) = \sum_{k=0}^{\lceil n^p \rceil} \frac{1}{n^p} \geq 1$.

The above shows that SFG_p and FG_p are not strongly equivalent. We will therefore compare these two distances in a slightly weaker manner by instead proving that they are topologically equivalent.

3.3.2 Equivalence of topologies

In this section, we prove that the topology of $\mathcal{D}^p(\Omega)$ endowed with SFG_p is the same as with FG_p . Note that in this specific subsection, our proof restrict to (possibly infinite) persistence diagrams instead of measures for the sake of simplicity. Extending the result to that more general setting is left for future work.

Theorem 2 (The topologies defined by SFG_p and FG_p are the same) *Let $\mu \in \mathcal{D}^p(\Omega)$ and $(\mu_n)_n$ be a sequence in $\mathcal{D}^p(\Omega)$. Then*

$$\mu_n \xrightarrow{\text{FG}_p} \mu \iff \mu_n \xrightarrow{\text{SFG}_p} \mu. \quad (79)$$

We will use the following characterisation of convergence in $(\mathcal{M}^p(\Omega), \text{FG}_p)$ from (Divol and Lacombe 2020),

$$\text{FG}_p(\mu_n, \mu) \rightarrow 0 \iff \begin{cases} \mu_n \xrightarrow{v} \mu \\ \text{Pers}_p(\mu_n) \rightarrow \text{Pers}_p(\mu) \end{cases} \quad (80)$$

Where $\mu_n \xrightarrow{v} \mu$ means that for all functions f with compact support in Ω , we have $\int_{\Omega} f(x) d\mu_n(x) \rightarrow \int_{\Omega} f(x) d\mu(x)$.

Proposition 10 *Let $\mu \in \mathcal{D}^p(\Omega)$ and $(\mu_n)_n$ be a sequence of $\mathcal{D}^p(\Omega)$ such that $\mu_n \xrightarrow{\text{FG}_p} \mu$ then $\mu_n \xrightarrow{\text{SFG}_p} \mu$.*

Proof If $p = 1$ this is simply a consequence and 1. For $p > 1$, we need to be slightly more precise.

Consider a sequence $\mu_n \in \mathcal{D}^p$ such that $\text{FG}_p(\mu_n, \mu) \rightarrow 0$ and let $\varepsilon > 0$. Because of (80), we therefore have $\mu_n \xrightarrow{v} \mu$ and in particular μ_n converges pointwise to μ . Hence, if we denote by γ_n the optimal transport plan achieving the infimum in $\text{FG}_p(\mu, \mu_n)$, for n large enough we know that if $\gamma(x, y) > 0$ then $d(x, y) < \varepsilon^2$. We will now bound the third term in 77. Let $A_{\geq \varepsilon} = \{(x, y) \in \Omega \times \Omega : d(x, \partial\Omega) \geq \varepsilon \text{ and } d(y, \partial\Omega) \geq \varepsilon\}$ and $A_{\leq \varepsilon} = \{(x, y) \in \Omega \times \Omega : d(x, \partial\Omega) \leq \varepsilon \text{ and } d(y, \partial\Omega) \leq \varepsilon\}$, we have

$$\iint_{\Omega \times \Omega} \frac{\min(d(x, \partial\Omega), d(y, \partial\Omega))^p}{\max(d(x, \partial\Omega), d(y, \partial\Omega))} d(x, y) d\gamma_n(x, y) \quad (81)$$

$$= \iint_{A_{\geq \varepsilon}} \frac{\min(d(x, \partial\Omega), d(y, \partial\Omega))^p}{\max(d(x, \partial\Omega), d(y, \partial\Omega))} d(x, y) d\gamma_n(x, y) \quad (82)$$

$$+ \iint_{A_{\leq 2\varepsilon}} \frac{\min(d(x, \partial\Omega), d(y, \partial\Omega))^p}{\max(d(x, \partial\Omega), d(y, \partial\Omega))} d(x, y) d\gamma_n(x, y) \quad (83)$$

$$\leq \varepsilon^2 \iint_{A_{\geq \varepsilon}} \frac{d(x, \partial\Omega)^p}{\inf_{(z, w) \in A_{\geq \varepsilon}} (d(z, \partial\Omega))} d\gamma_n(x, y) \quad (84)$$

$$+ \iint_{A_{\leq 2\varepsilon}} \min(d(x, \partial\Omega), d(y, \partial\Omega))^p d(x, \partial\Omega) d\gamma_n(x, y) \quad (85)$$

$$+ \iint_{A_{\leq 2\varepsilon}} \min(d(x, \partial\Omega), d(y, \partial\Omega))^p d(y, \partial\Omega) d\gamma_n(x, y) \quad (86)$$

$$\leq \varepsilon \text{Pers}_p(\mu_{\geq \varepsilon}) + \text{Pers}_p(\mu_{\leq 2\varepsilon}) + \text{Pers}_p(\mu_{n \leq 2\varepsilon}). \quad (87)$$

Now, using once again 80, we know that $\text{Pers}_p(\mu_{n \leq 2\varepsilon}) \rightarrow \text{Pers}_p(\mu_{\leq \varepsilon})$ and so we finally get that, for n sufficiently large,

$$\iint_{\Omega \times \Omega} \frac{\min(d(x, \partial\Omega), d(y, \partial\Omega))^p}{\max(d(x, \partial\Omega), d(y, \partial\Omega))} d(x, y) d\gamma_n(x, y) \leq \varepsilon(1 + \text{Pers}_p(\mu)) + 2\text{Pers}_p(\mu_{\leq \varepsilon}). \quad (88)$$

A similar bound can be obtained for the second term in 77. Combining these together yields the desired result i.e. that $\mu_n \xrightarrow{\text{SFG}_p} \mu$. \square

We now prove the converse implication. For this, we will show that the SFG_p convergence implies characterisation 80.

Proposition 11 *Let $\mu \in \mathcal{D}^p(\Omega)$ and $(\mu_n)_n$ be a sequence of $\mathcal{D}^p(\Omega)$ such that $\mu_n \xrightarrow{\text{SFG}_p} \mu$. Then $\text{Pers}_p(\mu_n) \rightarrow \text{Pers}_p(\mu)$.*

Proof From Proposition 3, we have $\text{SFG}_p(\nu, \emptyset) = \text{Pers}_p(\nu)$ for all $\nu \in \mathcal{M}^p(\Omega)$. The result then follows from the triangle inequality. \square

It remains to prove that the SFG_p convergence implies the vague convergence in duality with functions of $\mathcal{C}_c(\Omega)$. To do this, we will prove the pointwise convergence of the points of μ_n to the points of μ from which we will deduce the result using the fact that a compact of Ω only contains finitely many of those points.

Proposition 12 *Let $\mu \in \mathcal{D}^p(\Omega)$ and $(\mu_n)_n$ be a sequence of $\mathcal{D}^p(\Omega)$ such that $\mu_n \xrightarrow{\text{SFG}_p} \mu$. Then for all $x \in \text{spt}(\mu)$, there exists $\eta > 0$ such that for all $0 < \varepsilon < \eta$, $\mu_n(1_{B(x, \varepsilon)}) \rightarrow \mu(x)$*

To prove this result, we need the following technical lemma and definition.

Definition 3 Given $\varepsilon > 0$ and $x \in \Omega$, we denote by B_ε^x (or simply B_ε) the strip parallel to the diagonal of width 2ε and centered at x , by ∂B_ε its border and by $B_{\varepsilon, t} := B_\varepsilon \cap \Omega_t$.

Given $\mu \in \mathcal{M}^p(\Omega)$ and $C \subset \Omega$, we also define μ_C by $\mu_C(A) = \mu(A \cap C)$. Now, let $\mu, \nu \in \mathcal{M}^p(\Omega)$ and $C, D \subset \Omega$ we define

$$\tilde{\text{FG}}_{C, D}(\mu, \nu) := \inf_{\gamma \in \tilde{\text{Adm}}(\mu_C, \nu_D)} \iint_{\overline{C} \times \overline{D}} d(x, y)^p d\gamma(x, y), \quad (89)$$

where $\tilde{\text{Adm}}(\mu_C, \nu_D)$ is the set of Radon measures supported on $\overline{C} \times \overline{D}$ satisfying that, for all Borel subsets $A \subset C$ and $B \subset D$,

$$\gamma(A \times \overline{D}) = \mu_C(A) \quad \text{and} \quad \gamma(\overline{C} \times B) = \nu_D(B). \quad (90)$$

Eventually, we define

$$\tilde{\text{SFG}}_{C, D}(\mu, \nu) := \frac{1}{\sqrt{2}} \left(\int_{\mathbb{R}} \tilde{\text{FG}}_{C, D}^p(\pi_t \# \tilde{\mu}, \pi_t \# \tilde{\nu}) dt \right)^{\frac{1}{p}}. \quad (91)$$

Lemma 5 *Let $\mu, \nu \in \mathcal{M}^p(\Omega)$, for any $\varepsilon, \eta > 0$ and $x \in \Omega$ we have $\tilde{\text{SFG}}_{B_\varepsilon, B_\eta}(\mu, \nu) \leq \text{SFG}_p(\mu, \nu)$.*

Proof Let $\varepsilon, \eta > 0$ and $t \in \mathbb{R}$. We denote by γ_t one of the pullbacks of the optimal transport plan achieving the infimum in $\text{FG}_p(\pi_t \# \tilde{\mu}, \pi_t \# \tilde{\nu})$. We can then write

$$\iint_{\bar{\Omega} \times \bar{\Omega}} d(\pi_t(x), \pi_t(y))^p d\gamma_t(x, y) \quad (92)$$

$$\geq \iint_{B_\varepsilon \times B_\eta} d(\pi_t(x), \pi_t(y)) d\gamma_t(x, y) + \iint_{B_\varepsilon \times B_\eta^c \cup B_\varepsilon^c \times B_\eta} d(\pi_t(x), \pi_t(y)) d\gamma_t(x, y) \quad (93)$$

(94)

$$\geq \iint_{B_\varepsilon \times B_\eta} d(\pi_t(x), \pi_t(y)) d\gamma_t(x, y) + \iint_{B_\varepsilon \times B_\eta^c} d(\pi_t(x), \partial B_\eta) d\gamma_t(x, y) \quad (95)$$

$$+ \iint_{B_\varepsilon^c \times B_\eta} d(\partial B_\varepsilon, \pi_t(y)) d\gamma_t(x, y) \quad (96)$$

$$= \iint_{\bar{B}_\varepsilon \times \bar{B}_\eta} d(\pi_t(x), \pi_t(y)) \tilde{\gamma}_t(x, y), \quad (97)$$

where we set

$$\tilde{\gamma}_t(x, y) = \begin{cases} \gamma_t(x, y) & \text{if } x, y \in B_\varepsilon \times B_\eta \\ \int_{z \in B_\eta^c} d\gamma_t(x, z) & \text{if } x \in B_\varepsilon \text{ and } y = \partial B_\eta \\ \int_{z \in B_\varepsilon^c} d\gamma_t(z, y) & \text{if } x = \partial B_\varepsilon \text{ and } y \in B_\eta. \end{cases} \quad (98)$$

It is then easy to check that $\pi_t \# \tilde{\gamma}_t \in \tilde{\text{Adm}}(\pi_t \# \tilde{\mu}_{B_\varepsilon}, \pi_t \# \tilde{\nu}_{B_\eta})$ for all $t \in \mathbb{R}$ which concludes. \square

Lemma 6 Let $I \subset \mathbb{R}$, $\mu, \nu \in \mathcal{D}^p(\Omega)$ and $x \in \Omega$. For any $t \in \mathbb{R}$ and $\varepsilon > 0$, let $\Delta_t := \tilde{\nu}(B_{\varepsilon/2, t}) - \tilde{\mu}(B_{\varepsilon/2, t})$.

There exists $\eta > 0$ depending only on μ and x , such that for all $0 < \varepsilon < \eta$ and $C > 0$, if $\Delta_t > C$ for all $t \in I$ then

$$\tilde{\text{SFG}}_{B_{\varepsilon/2}, B_\varepsilon}(\nu, \mu) \geq C|I|\varepsilon/2. \quad (99)$$

Proof Since there are only finitely many points of μ in $B_{d(x, \partial\Omega)/2}$, there exists $\eta > 0$ verifying $\text{spt}(\mu) \cap B_\eta \subset D_x := \{z \in \Omega : d(z, \partial\Omega) = d(x, \partial\Omega)\}$. Let $0 < \varepsilon < \eta$. We have

$$\tilde{\text{SFG}}_{B_{\varepsilon/2}, B_\varepsilon}(\nu, \mu) \geq \int_I \tilde{\text{FG}}_{B_{\varepsilon/2}, B_\varepsilon}(\pi_t \# \tilde{\nu}, \pi_t \# \tilde{\mu}) dt \quad (100)$$

$$\geq \int_I \Delta_t \times \varepsilon/2 dt \quad (101)$$

$$\geq C|I|\varepsilon/2. \quad (102)$$

The second inequality comes from the fact that since $|\Delta_t| > C$ there are two cases:

1. if $\Delta_t > C$, then at least C amount of mass of ν needs to be transported from $B_{\varepsilon/2}$ to ∂B_ε hence a cost of at least $\varepsilon/2$,
2. if $\Delta_t < -C$, then at least C amount of mass of μ needs to be transported from D_x to $\partial B_{\varepsilon/2}$ hence a cost of $\varepsilon/2$.

\square

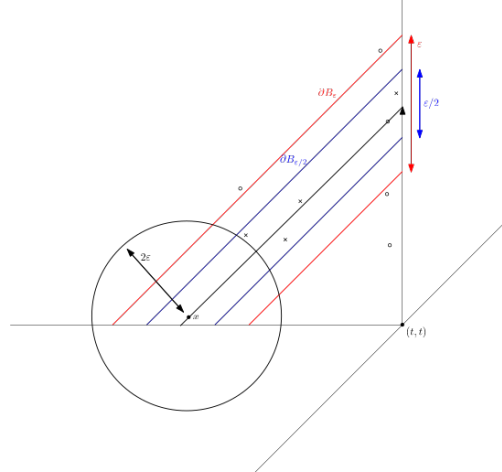


Fig. 3: $B_{\varepsilon/2}$ (blue) and B_{ε} (red)

We can now prove Proposition 12. For the sake of simplicity we will assume $p = 1$ but the argument can easily be adapted to the general case.

Proof First step: $\liminf \mu_n(1_{B(x, \varepsilon)}) \geq \mu(x)$

Suppose for a contradiction that there exists $x \in \text{spt}(\mu)$ such that for all $\eta > 0$ there exists $0 < \varepsilon < \eta$ satisfying that for infinitely many μ_n we have $\mu_n(1_{B(x, 2\varepsilon)}) < \mu(x)$. Let η be given by Lemma 6 and $0 < \varepsilon < \eta$. By further reducing η , we can assume that $\text{spt}(\mu) \cap B_\eta \subset D_x := \{z \in \Omega : d(z, \partial\Omega) = d(x, \partial\Omega)\}$ and that the minimal distance between two points of $D_x \cap \text{spt}(\mu)$ is at least 2ε . Since according to Lemma 5 we have $\tilde{\text{SFG}}_{\varepsilon/2, \varepsilon}(\mu_n, \mu) \leq \text{SFG}(\mu_n, \mu)$ we will lower bound $\tilde{\text{SFG}}_{B_{\varepsilon/2}, B_\varepsilon}(\mu_n, \mu)$ (which we will denote simply by SFG for short) to obtain a contradiction.

In the rest of the proof, we use the result of Lemma 6 repeatedly to study more extensively the quantity Δ_t (introduced in the same lemma) and reach a contradiction. Also, all points of $\text{spt}(\tilde{\mu}_n) \cap B_{\varepsilon/2}$ do not have the same mass (they range between $\frac{1}{d(x, \partial\Omega) + \varepsilon}$ and $\frac{1}{d(x, \partial\Omega) - \varepsilon}$). However, since $\text{Pers}_p(\mu_n) \rightarrow \text{Pers}_p(\mu)$, the sequence $\tilde{\mu}_n(B_{\varepsilon/2})$ is uniformly bounded by some $M > 0$ and hence one can show that Δ_t lies within $\frac{2M\varepsilon}{d(x, \partial\Omega)^2}$ of the nearest integer multiple of $1/d(x, \partial\Omega)$. As such, by possibly shrinking η further, this quantity can be assumed to be smaller than $\delta := \frac{1}{4d(x, \partial\Omega)}$.

Observe that for $t \in [x_2 - \varepsilon, x_2 + \varepsilon]$, at most $\mu(x) - 1$ points (counting multiplicities) of μ_n "disappear" from $B_{\varepsilon/2, t}$ (that is are contained in $B_{\varepsilon/2, x_2 - \varepsilon}$ but not in $B_{\varepsilon/2, x_2 + \varepsilon}$) and during this interval, the only point of μ leaving $B_{\varepsilon/2, t}$ is x (of multiplicity $\mu(x)$). Then, during that same interval, only one point of μ can appear in $B_{\varepsilon/2, t}$ which we will denote by y . We distinguish several cases:

1. At $t_0 = x_2 - \varepsilon$, $|\Delta_{t_0}| \leq \delta$. We then distinguish 3 cases depending on when y appears.
 - (a) If y never appears, then since x disappears at $t = x_2$ and at most $\mu(x) - 1$ points of μ_n (counting multiplicities) disappear between $t = x_2 - \varepsilon$ and $t = x_2 + \varepsilon$

we have $\Delta_t \geq 1/d(x, \partial\Omega) - \delta$ for $t \in [x_2, x_2 + \varepsilon]$ and therefore, according to Lemma 6, $\tilde{SW}(\mu_n, \mu) \geq \frac{\varepsilon^2}{2} \left(\frac{1}{d(x, \partial\Omega)} - \delta \right)$.

- (b) Then, if y appears before $x_2 - \varepsilon/4$, $\mu(y)$ points of μ_n must appear before x_2 otherwise $\Delta_t \leq -1/d(x, \partial\Omega) + \delta$ for $t \in [x_2 - \varepsilon/4, x_2]$. So we again have $\Delta_t \geq 1/d(x, \partial\Omega) - \delta$ for $t \in [x_2, x_2 + \varepsilon]$ hence $\tilde{SW}(\mu_n, \mu) \geq \frac{\varepsilon^2}{2} \left(\frac{1}{d(x, \partial\Omega)} - \delta \right)$. The case where y appears after $x_2 + \varepsilon/4$ is handled similarly.
- (c) If y appears between $x_2 - \varepsilon/4$ and $x_2 + \varepsilon/4$. Then, if $\mu(y)$ points of μ_n or more appear between $x_2 - 3\varepsilon/4$ and $x_2 + 3\varepsilon/4$, we get this time $\tilde{SW} \geq \frac{\varepsilon^2}{8} \left(\frac{1}{d(x, \partial\Omega)} - \delta \right)$ since in that case we would have $\Delta_t \geq 1/d(x, \partial\Omega) - \delta$ between $x_2 + 3\varepsilon/4$ and $x_2 + \varepsilon$ (this is because the distance between two points of $D_x \cap \text{spt}(\mu)$ is at least ε). As such less than $\mu(y)$ points of μ_n appear between $x_2 - 3\varepsilon/4$ et $x_2 + 3\varepsilon/4$. In other words, y verifies the same hypothesis as x but with $\varepsilon/2$ instead of 2ε i.e. $\mu_n(1_{B(y, \varepsilon/2)}) < \mu(y)$.
- 2. If at $t_0 = x_2 - \varepsilon$, $|\Delta_{t_0}| \geq \delta$, then there exists $\varepsilon' \in [3\varepsilon/4, \varepsilon]$ such that $|\Delta_{x_2 - \varepsilon'}| \leq \delta$. We are thus reduced to the previous case and we get that the point y (if it exists) verifies $\mu_n(1_{B(y, \varepsilon'/4)}) < \mu(y)$ and so in particular $\mu_n(1_{B(y, \varepsilon/4)}) < \mu(y)$.

Setting $N := |D_x \cap \text{supp}(\mu)|$, it follows, by iteration, that $\tilde{SW}(\mu_n, \mu) \geq \left(\frac{1}{8} \right)^{2N} \frac{\varepsilon^2}{2} \left(\frac{1}{d(x, \partial\Omega)} - \delta \right)$. And so we deduce that $SW_p(\mu_n, \mu) \not\rightarrow 0$ which is the desired contradiction. Hence, for all sufficiently large n , we have $\mu_n(1_{B(x, \varepsilon)}) \geq \mu(x)$.

Second step: $\limsup \mu_n(1_{B(x, \varepsilon)}) \leq \mu(x)$:

Suppose for a contradiction that, up to extracting a subsequence of (μ_n) , there exist sequences $(a_{i,n})_{1 \leq i \leq k}$ of points of $\text{spt}(\mu_n)$ such that $a_{i,n} \xrightarrow[n \rightarrow +\infty]{} x$, the $a_{i,n}$ are all distincts and $\sum_{i=1}^k \mu_n(a_{i,n}) > \mu(x)$ for all $n \in \mathbb{N}$. Like above, we consider the problem SFG associated to the regions B_ε and $B_{\varepsilon/2}$ where we assume ε is small enough so that the only points of $B_\varepsilon \cap \text{spt}(\mu)$ are in D_x and the distance between two points of $D_x \cap \text{spt}(\mu)$ is at least 2ε . We then fix N large enough to have $d(a_{i,n}, x) \leq \varepsilon/4$ for all $n \geq N$ and all $1 \leq i \leq k$. Furthermore, using the result of the first step, for all $z \in D_x$, we may find sequences $(z_{i,n})_{1 \leq i \leq k_z}$ such that $z_{i,n} \rightarrow z$, the $z_{i,n}$ are all distincts and $\sum_{i=1}^{k_z} m_{\mu_n}(z_{i,n}) \geq \mu(z)$ for all $n \in \mathbb{N}$. Hence, we can assume that $d(z_{i,n}, z) \leq \varepsilon/4$ for all $z \in D_x$, $1 \leq i \leq k_z$ and $n \geq N$ (which is possible because $D_x \cap \text{spt}(\mu)$ is finite).

In that setting, with $t_0 = x_2 - \varepsilon$, to any point $z \in (D_x \cap B_{\varepsilon/2, t_0}) \setminus \{x\}$ except eventually the "last" (that is the one with the highest z_2 coordinate) corresponds at least $\mu(z)$ points (counting multiplicities) in $B_{\varepsilon/2, t_0}$ (the $z_{i,n}$ we defined above). To those are added the $\mu(x) + 1$ points associated to x since we are arguing by contradiction. In particular, from this we deduce that if $\Delta_{t_0} \leq \delta$, the last point y of $\text{spt}(\mu) \cap B_{\varepsilon, t}$ appeared between $t_0 - \varepsilon/4$ and t_0 . We then have

- If $\Delta_{t_0} \leq \delta$, then (as explained above) the last point y of $\text{spt}(\mu) \cap B_{\varepsilon, t}$ appeared between $t_0 - \varepsilon/4$ and t_0 and as such the corresponding points $y_{i,n}$ must appear before $t_0 + \varepsilon/4$. We then have $\Delta_t \geq \frac{1}{d(x, \partial\Omega)} - \delta$ for $x_2 - 3\varepsilon/4 \leq t \leq x_2 - \varepsilon/4$ which is not possible.
- If $\Delta_{t_0} \geq \frac{1}{d(x, \partial\Omega)} - \delta$, then necessarily a point y of μ appears before $t = x_2 - 3\varepsilon/4$. But then again, the associated points $y_{i,n}$ appear before $t = x_2 - \varepsilon/2$. However no

other point of $\text{spt}(\mu)$ can appear before $x_2 - \varepsilon/4$ and as such $\Delta_t \geq 1/d(x, \partial\Omega) - \delta$ for $x_2 - \varepsilon/2 \leq t \leq x_2 - \varepsilon/4$ hence $\tilde{\text{SW}} \geq \frac{\varepsilon^2}{8} \left(\frac{1}{d(x, \partial\Omega)} - \delta \right)$.

Finally, for all $x \in \text{spt}(\mu)$, there exists $\eta > 0$ such that for all $\eta > \varepsilon > 0$ we have $\mu_n(1_{B(x, \varepsilon)}) \rightarrow \mu(x)$. \square

We finally get the following result.

Proposition 13 *Let $\mu \in \mathcal{D}^p(\Omega)$ and $(\mu_n)_n$ be a sequence of $\mathcal{D}^p(\Omega)$ such that $\mu_n \xrightarrow{\text{SFG}_p} \mu$. Then $\mu_n \xrightarrow{v} \mu$.*

Proof This is a direct consequence of Proposition 12 and the fact that any compact set of Ω contains finitely many points of $\text{spt}(\mu)$. \square

And hence the converse implication in Theorem 2 holds.

4 Numerical considerations and experimental results

In this section, we introduce algorithms for computing the Sliced Figalli–Gigli distance, and the associated kernel (SFGK), both in exact and approximate forms. We then evaluate their empirical performance on standard machine learning tasks, using the same benchmark datasets as those considered for the Sliced Wasserstein kernel on persistence diagrams proposed by Carrière et al. (Carrière et al. 2017). Owing to the close similarity between the two kernels, we do not anticipate substantial differences in practical performance, a hypothesis that is confirmed by our numerical experiments. Accordingly, the goal of this section is not to claim a systematic empirical advantage over the SWK of (Carrière et al. 2017), but rather to demonstrate that the stronger theoretical foundations underpinning SFGK do not come at the expense of numerical efficiency or predictive performance.

4.1 Exact and approximated computation of the SFG distance

In this section we give algorithms to compute both the exact value and approximations of SFG.

This algorithm works since the value of $\text{FG}_p(\pi_t \# \tilde{X}, \pi_t \# \tilde{Y})$ does not change between two consecutive events. It computes the exact SFG_p distance between the two inputted diagrams in $\mathcal{O}((N_1 + N_2) \times \max(N_1, N_2))$ where N_1 and N_2 are the number of points in each diagram. This is essentially optimal if N_1 and N_2 are roughly the same size since the above algorithm needs to compute the matrix of the distances between points of X and points of Y (any point of X may be transported onto any point of Y) which can only be done in $\mathcal{O}(N_1 \times N_2)$. We can also compute an approximation of the SFG_p distance by simply approximating the outer integral, as detailed in Section 4.1.

It is sufficient to sample the values t_1, \dots, t_k between $\min(\{x_{i,1}, 1 \leq i \leq N_1\} \cup \{y_{j,1}, 1 \leq j \leq N_2\})$ and $\max(\{x_{i,2}, 1 \leq i \leq N_1\} \cup \{y_{j,2}, 1 \leq j \leq N_2\})$ since $\text{FG}_p(\pi_t \# \tilde{X}, \pi_t \# \tilde{Y}) = 0$ outside of these bounds. We considered sampling the t_i , either

Algorithm 1 Exact computation of SFG_p

Input: Two diagrams $X = \{x_1, \dots, x_{N_1}\}$, $Y = \{y_1, \dots, y_{N_2}\}$
Sort $\{x_{1,1}, x_{1,2}, \dots, x_{N_1,1}, x_{N_1,2}, y_{1,1}, \dots, y_{N_2,2}\}$ into a list of events E .
Initialize $\text{SFG} = 0$ and two binary search trees $X_t = \{\}$, $Y_t = \{\}$
for $i = 1, \dots, 2(N_1 + N_2)$ **do**
 if $E[i]$ is of the form $z_{j,1}$ **then**
 $Z_t \leftarrow Z_t + \{z_j\}$
 else
 $Z_t \leftarrow Z_t - \{z_j\}$
 end if
 Iterate over X_t and Y_t to compute $\alpha = \text{FG}_p(\pi_t \# \tilde{X}, \pi_t \# \tilde{Y})$
 $\text{SFG} \leftarrow \text{SFG} + (E[i+1] - E[i])\alpha$
end for
Output: SFG

Algorithm 2 Approximate computation of SFG_p

Input: Two diagrams $X = \{x_1, \dots, x_{N_1}\}$, $Y = \{y_1, \dots, y_{N_2}\}$ and an integer k
Sort X and Y with respect to $d(\cdot, \partial\Omega)$
Samples values t_1, \dots, t_k between $\min(\{x_{i,1}, 1 \leq i \leq N_1\} \cup \{y_{j,1}, 1 \leq j \leq N_2\})$ and
 $\max(\{x_{i,2}, 1 \leq i \leq N_1\} \cup \{y_{j,2}, 1 \leq j \leq N_2\})$
Initialize $\text{SFG} = 0$
for $i = 1, \dots, k$ **do**
 Compute $X_t := X \cap \Omega_t$ and $Y_t := Y \cap \Omega_t$
 Iterate over X_t and Y_t to compute $\alpha = \text{FG}_p(\pi_{t_i} \# \tilde{X}, \pi_{t_i} \# \tilde{Y})$
 $\text{SFG} \leftarrow \text{SFG} + (t_i - t_{i-1})\alpha$
end for
Output: SFG

uniformly or by sampling from a Gaussian KDE fitted on the different event values (as defined in the previous algorithm). In practice, we found that the uniform sampling lead to better convergence speed (see Figure 4). The above algorithm runs in $\mathcal{O}(N_1(\log(N_1) + k) + N_2(\log(N_2) + k))$ since computing $\text{FG}_p(\pi_t \# \tilde{X}, \pi_t \# \tilde{Y})$ can be done in $\mathcal{O}((N_1 + N_2)k)$.

Remark 8 In the above algorithm, the sampled values depend on the input diagrams. This allows to avoid sampling values where $\text{FG}_p(\pi_t \# \tilde{X}, \pi_t \# \tilde{X})$ is trivially zero. However, by doing that, this approximation of SFG_p is not CND. If one wants to ensure this property still holds when computing approximation of SFG_p the sampled values need to be fixed ahead of time. For example, when computing a Gram matrix of diagrams with the SFG kernel the sampled values used must be the same for all the distance computations or the resulting matrix might not be PSD. In practice, we found that when training an SVM the resulting matrix were close enough to being PSD for it to not cause convergence issues.

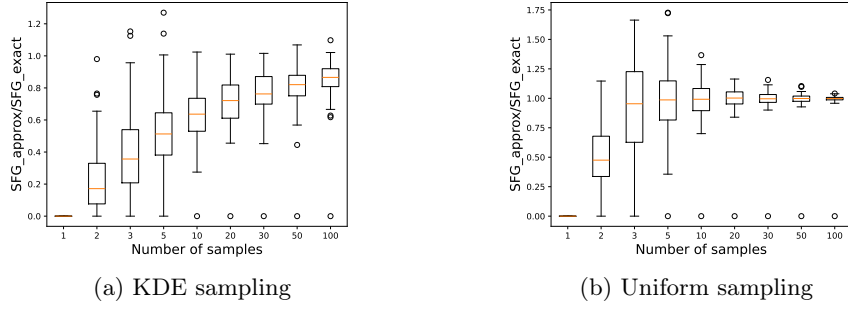


Fig. 4: Boxplot of the ratio between the approximation of SFG and its exact value with respect to the number of samples used for the approximation. The persistence diagrams we used to get this plot were taken from the *Orbits* dataset we generated (see Section 4.3). The uniform sampling leads to better convergence speeds while the gaussian KDE sampling tends to underestimate the value of SFG.

Remark 9 We also have very similar algorithms to compute exact and approximate values of the variant $\widehat{\text{SFG}}$ described in Appendix A which we do not detail here. They run in respectively $\mathcal{O}(N_1 N_2 \times \max(N_1, N_2))$ and $\mathcal{O}(N_1(\log(N_1) + k) + N_2(\log(N_2) + k))$.

4.2 Tightness of theoretical bounds between FG and SFG

We explore numerically how tight the bound of Theorem 1 is. For this purpose, we compute the ratio between the SFG distance between persistence diagrams sampled either (a) uniformly⁴, (b) from the *Orbits* dataset or (c) from the *Outex* dataset (see Section 4.3) and the theoretical bound given by Theorem 1. The results are given in Fig. 5.

We observe that the theoretical bound seems relatively tight for $p \neq 1$ as evidenced in 5b. For $p = 1$ we empirically observe that $0.2 \lesssim \frac{\text{SFG}_1}{3\text{FG}_1} \lesssim 0.4$, i.e. $0.6\text{FG}_1 \lesssim \text{SFG}_1 \lesssim 1.2\text{FG}_1$. Even though we know it is not possible to obtain a lower bound of the form $C \cdot \text{SFG}_1 \leq \text{FG}_1$ for all persistence diagrams by considering peculiar adversarial examples, we observe that such a bound seems to hold for diagrams actually encountered in applications.

4.3 Experimental results on classification tasks

We tested the two distances SFG_1 and $\widehat{\text{SFG}}_1$ (simply denoted SFG and $\widehat{\text{SFG}}$ below, where we recall that $\widehat{\text{SFG}}$ refers to the variant of SFG using a different projection onto the geodesics, presented in Appendix A) against the Sliced Wasserstein distance (SW, see section 2.4) on two different experiments proposed in (Carrière et al. 2017). For both of those, we train classifiers using the LIBSVM implementation (Chang and Lin 2011) of C -SVM and average the results over 5 runs. We cross-validate the cost

⁴That is, persistence diagrams each consisting of 100 points sampled uniformly on $[0, 1]^2$.

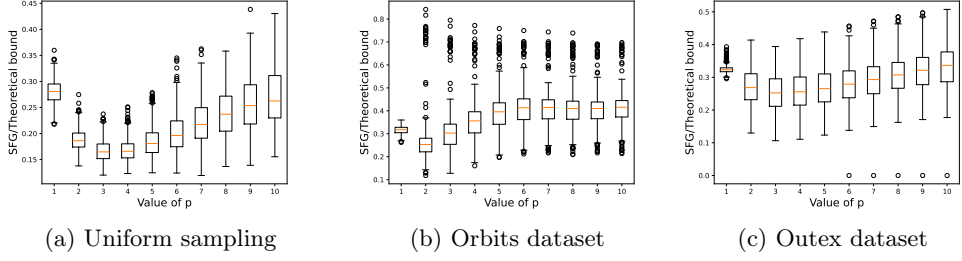


Fig. 5: Boxplot of the ratio between SFG and the theoretical bound of Theorem 1 for different values of p . For each value of p , the boxplot was obtained with 500 persistence diagrams which were sampled uniformly for (a) and using the procedures described in Section 4.3 for (b) and (c).

factor over the grid $\{0.01, 0.1, 1.0, 10.0, 100.0\}$. All the distance functions we consider only have one parameter: the bandwidth σ . When training, we choose it by 5-fold cross-validation among 15 different values that we obtain by multiplying the first decile, last decile and median of the Gram matrix values of the training set by the following factors: $\{0.01, 0.1, 1.0, 10.0, 100.0\}$. We use 20 directions to approximate SW and sample 20 values to approximate SFG and $\widehat{\text{SFG}}$.

4.3.1 Orbit recognition

Dataset This task is based on the *linked twist map* discrete dynamical system. Given initial positions $(x_0, y_0) \in [0, 1]^2$ and a parameter $r > 0$ its orbits can be computed with the following equations:

$$\begin{cases} x_{n+1} = x_n + ry_n(1 - y_n) \mod 1 \\ y_{n+1} = y_n + rx_{n+1}(1 - x_{n+1}) \mod 1 \end{cases} \quad (103)$$

The orbits exhibit very different behaviour depending on the values of the parameter r . For example, as can be seen in Figure 5, when $r = 3.5$ there seems to be no specific structure whereas for $r = 4.1$ a void appears in the center.

Following what was done in (Carrière et al. 2017), we use 5 parameter values $r \in \{2.5, 3.5, 4, 4.1, 4.3\}$ and for each of those we generate 100 orbits with 1000 points and random initial positions. We then use the GUDHI library (The GUDHI Project 2025) to compute the persistence diagrams of the distance to the points and use them (in homological dimension 1) to produce an orbit classifier by training over a 60%-40% train-test split of the data.

Results. As reported in Table 1 both SFG and $\widehat{\text{SFG}}$ achieve a performance similar to the one of the Sliced Wasserstein Kernel.

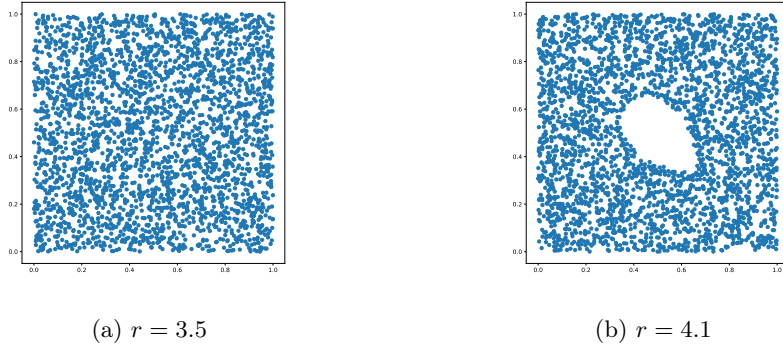


Fig. 6: Two orbits with different parameter values, the classifier is trained to predict the value of the parameter.

4.3.2 Texture classification

Dataset. The second experiment uses the *OUTEX* database for texture classification. Since we were unable to access the original *OUTEX0000* dataset we instead use part of an extended version of it: *Outex_TC_00010-r* (available at <https://color.univ-lille.fr/datasets/extended-outex>). For each of the images in the database we compute the sign component of the CLPB descriptor (Guo et al. 2010) with radius $R = 1$ and neighbours $P = 8$. The output of this descriptor can then be interpreted as a weighted cubical cell complex (Reininghaus et al. 2015) from which we again compute a persistence diagram using the GUDHI library. We then use it in homological dimension 0 to produce a classifier over a 50%-50% train-test split of the data.

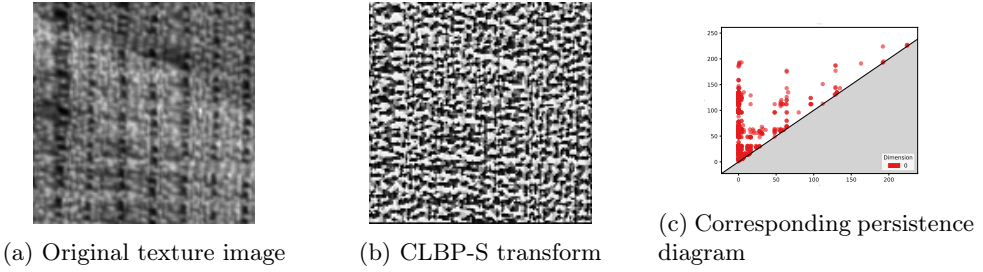


Fig. 7: The pipeline we use to produce texture classifiers.

Results: As reported in Table 1 both SFG and $\widehat{\text{SFG}}$ again achieve a performance similar to the one of the Sliced Wasserstein Kernel.

TASK	SW	SFG	SFG
ORBIT	79.7 ± 1.64	80.8 ± 1.2	79.8 ± 0.4
TEXTURE	89.5 ± 5.2	90.1 ± 1.3	91.7 ± 2.8

Table 1: Accuracies on the two different experiments we performed: Orbits and Textures.

5 Conclusion

In this work, we defined a new distance between persistence diagrams that remains faithful to the geometry of the space of PDs while being computationally efficient. Unlike the Sliced Wasserstein distance, the Sliced Figalli–Gigli distance admits a natural extension to infinite persistence diagrams and to persistence measures, placing it in a broader and more flexible measure-theoretic framework that encompasses existing finite-diagram formulations as special cases.

Left open by our work are several directions for future research. On the theoretical side, while we derive in Section 3.3 stability bounds for the SFG distance, empirical results (see Section 4.2) suggest that the observed stability in practical settings is significantly stronger. Understanding this gap, for instance by identifying refined assumptions on the distributions of persistence diagrams considered under which improved bounds can be established, is an interesting direction for further investigation. Following recent advances in the computational optimal transport literature, one may also consider variants of the SFG distance, e.g. using a maximum instead of an integration (Deshpande et al. 2019; Kolouri et al. 2019). Another appealing question—going beyond Topological Data Analysis—would be to generalize the SFG distance to domains more general than the open half-plane Ω . Indeed, in this work, the (somewhat simple) geometry of Ω and of the resulting geodesics emanating from $\partial\Omega$ was crucial (and sufficient for our purpose). However, the seminal formalism introduced by Figalli and Gigli in (Figalli and Gigli 2010) enable more general domains $(\Omega, \partial\Omega)$ (e.g. $\bar{\Omega}$ being a compact subset of \mathbb{R}^d and its boundary $\partial\Omega$ being reasonably smooth); defining a sliced Figalli–Gigli distance in that cases would be of interest.

References

Aukerman, A., Carrière, M., Chen, C., Gardner, K., Rabadán, R., Vanguri, R.: Persistent Homology Based Characterization of the Breast Cancer Immune Microenvironment: A Feasibility Study. *Journal of Computational Geometry (JoCG)* **12**(2), 183–206 (2021)

Adams, H., Emerson, T., Kirby, M., Neville, R., Peterson, C., Shipman, P., Chepushtanova, S., Hanson, E., Motta, F., Ziegelmeier, L.: Persistence images: A stable vector representation of persistent homology. *Journal of Machine Learning Research* **18**(8), 1–35 (2017)

Bukkuri, A., Andor, N., Darcy, I.K.: Applications of topological data analysis in oncology. *Frontiers in artificial intelligence* **4**, 659037 (2021)

Botnan, M., Crawley-Boevey, W.: Decomposition of persistence modules. *Proceedings of the American Mathematical Society* **148**(11), 4581–4596 (2020)

Bonet, C., Chapel, L., Drumetz, L., Courty, N.: Hyperbolic sliced-wasserstein via geodesic and horospherical projections. In: *Topological, Algebraic and Geometric Learning Workshops 2023*, pp. 334–370 (2023). PMLR

Berg, C., Christensen, J.P.R., Ressel, P.: General Results on Positive and Negative Definite Matrices and Kernels, pp. 66–85. Springer, New York, NY (1984). https://doi.org/10.1007/978-1-4612-1128-0_3

Bonet, C., Drumetz, L., Courty, N.: Sliced-wasserstein distances and flows on cartan-hadamard manifolds. *Journal of Machine Learning Research* **26**(32), 1–76 (2025)

Bubenik, P., Elchesen, A.: Virtual persistence diagrams, signed measures, wasserstein distances, and banach spaces. *Journal of Applied and Computational Topology* **6**(4), 429–474 (2022)

Berwald, J.J., Gottlieb, J.M., Munch, E.: Computing wasserstein distance for persistence diagrams on a quantum computer. *arXiv preprint arXiv:1809.06433* (2018)

Bonet, C., Malézieux, B., Rakotomamonjy, A., Drumetz, L., Moreau, T., Kowalski, M., Courty, N.: Sliced-wasserstein on symmetric positive definite matrices for m/eeg signals. In: *International Conference on Machine Learning*, pp. 2777–2805 (2023). PMLR

Boedihardjo, M.T.: Sharp bounds for max-sliced wasserstein distances. *Foundations of Computational Mathematics*, 1–32 (2025)

Bonet, C.: Leveraging Optimal Transport via Projections on Subspaces for Machine Learning Applications. PhD thesis, Université de Bretagne Sud (2023)

Bubenik, P.: Statistical topological data analysis using persistence landscapes. *Journal*

of Machine Learning Research **16**(3), 77–102 (2015)

Bubenik, P., Wagner, A.: Embeddings of persistence diagrams into hilbert spaces. Journal of Applied and Computational Topology **4**(3), 339–351 (2020) <https://doi.org/10.1007/s41468-020-00056-w>

Carrière, M., Cuturi, M., Oudot, S.: Sliced Wasserstein kernel for persistence diagrams. In: Precup, D., Teh, Y.W. (eds.) Proceedings of the 34th International Conference on Machine Learning. Proceedings of Machine Learning Research, vol. 70, pp. 664–673 (2017). <https://proceedings.mlr.press/v70/carriere17a.html>

Chazal, F., Divol, V.: The density of expected persistence diagrams and its kernel based estimation. In: SoCG 2018-Symposium of Computational Geometry (2018)

Chazal, F., Silva, V., Glisse, M., Oudot, S.: The Structure and Stability of Persistence Modules, (2016)

Chung, Y.-M., Hu, C.-S., Sun, E., Tseng, H.C.: Morphological Multiparameter Filtration and Persistent Homology in Mitochondrial Image Analysis. PLoS One **19**(9), 0310157 (2024)

Chang, C.-C., Lin, C.-J.: Libsvm: A library for support vector machines. ACM Trans. Intell. Syst. Technol. **2**(3) (2011) <https://doi.org/10.1145/1961189.1961199>

Cao, Y., Monod, A.: Approximating persistent homology for large datasets. arXiv preprint arXiv:2204.09155 (2022)

Chazal, F., Oudot, S.Y., Glisse, M., Silva, V.: The Structure and Stability of Persistence Modules. SpringerBriefs in Mathematics, p. 116 (2016). <https://doi.org/10.1007/978-3-319-42545-0> . <https://inria.hal.science/hal-01330678>

Carrière, M., Oudot, S., Ovsjanikov, M.: Stable Topological Signatures for Points on 3D Shapes. Computer Graphics Forum **34**(5), 1–12 (2015)

Deshpande, I., Hu, Y.-T., Sun, R., Pyrros, A., Siddiqui, N., Koyejo, S., Zhao, Z., Forsyth, D., Schwing, A.G.: Max-sliced wasserstein distance and its use for gans. In: Proceedings of the IEEE/CVF Conference on Computer Vision and Pattern Recognition, pp. 10648–10656 (2019)

Divol, V., Lacombe, T.: Understanding the topology and the geometry of the space of persistence diagrams via optimal partial transport. Journal of Applied and Computational Topology **5**, 1–53 (2020)

Divol, V., Lacombe, T.: Estimation and quantization of expected persistence diagrams. In: International Conference on Machine Learning, pp. 2760–2770 (2021). PMLR

Deshpande, I., Zhang, Z., Schwing, A.G.: Generative modeling using the sliced wasserstein distance. In: Proceedings of the IEEE Conference on Computer Vision and

Pattern Recognition, pp. 3483–3491 (2018)

Edelsbrunner, H., Harer, J.: Computational Topology: an Introduction, (2010)

Figalli, A., Gigli, N.: A new transportation distance between non-negative measures, with applications to gradients flows with dirichlet boundary conditions. *Journal de Mathématiques Pures et Appliquées* **94**, 107–130 (2010)

Feragen, A., Lauze, F., Hauberg, S.: Geodesic exponential kernels: When curvature and linearity conflict. In: 2015 IEEE Conference on Computer Vision and Pattern Recognition (CVPR), pp. 3032–3042 (2015). <https://doi.org/10.1109/CVPR.2015.7298922>

The GUDHI Project: GUDHI User and Reference Manual, 3.11.0 edn. (2025). The GUDHI Project. <https://gudhi.inria.fr/doc/3.11.0/>

Guo, Z., Zhang, L., Zhang, D.: A completed modeling of local binary pattern operator for texture classification. *IEEE Transactions on Image Processing* **19**(6), 1657–1663 (2010) <https://doi.org/10.1109/TIP.2010.2044957>

Hiraoka, Y., Nakamura, T., Hirata, A., Escolar, E.G., Matsue, K., Nishiura, Y.: Hierarchical Structures of Amorphous Solids Characterized by Persistent Homology. *Proceedings of the National Academy of Sciences* **113**(26), 7035–7040 (2016)

Kusano, G., Fukumizu, K., Hiraoka, Y.: Kernel method for persistence diagrams via kernel embedding and weight factor. *Journal of Machine Learning Research* **18**(189), 1–41 (2018)

Kusano, G., Hiraoka, Y., Fukumizu, K.: Persistence weighted gaussian kernel for topological data analysis. In: Balcan, M.F., Weinberger, K.Q. (eds.) *Proceedings of The 33rd International Conference on Machine Learning. Proceedings of Machine Learning Research*, vol. 48, pp. 2004–2013. PMLR, New York, New York, USA (2016). <https://proceedings.mlr.press/v48/kusano16.html>

Kolouri, S., Nadjahi, K., Simsekli, U., Badeau, R., Rohde, G.: Generalized sliced wasserstein distances. *Advances in neural information processing systems* **32** (2019)

Kolouri, S., Zou, Y., Rohde, G.K.: Sliced wasserstein kernels for probability distributions. In: *Proceedings of the IEEE Conference on Computer Vision and Pattern Recognition*, pp. 5258–5267 (2016)

Nadjahi, K.: Sliced-wasserstein distance for large-scale machine learning: theory, methodology and extensions. PhD thesis, Institut polytechnique de Paris (2021)

Nadjahi, K., Durmus, A., Chizat, L., Kolouri, S., Shahrampour, S., Simsekli, U.: Statistical and topological properties of sliced probability divergences. *Advances in Neural Information Processing Systems* **33**, 20802–20812 (2020)

Olejniczak, M., Tierny, J.: Topological Data Analysis of Vortices in the Magnetically-Induced Current Density in LiH Molecule. *Physical Chemistry Chemical Physics* **25**(8), 5942–5947 (2023)

Oudot, S.: Persistence Theory: From Quiver Representations to Data Analysis vol. 209, (2015)

Peyré, G., Cuturi, M.: Computational Optimal Transport (2020). <https://arxiv.org/abs/1803.00567>

Park, S., Slepčev, D.: Geometry and analytic properties of the sliced wasserstein space. *Journal of Functional Analysis* **289**(7), 110975 (2025)

Pascucci, V., Tricoche, X., Hagen, H., Tierny, J.: Topological Methods in Data Analysis and Visualization: Theory, Algorithms, and Applications. Springer, ??? (2010)

Reininghaus, J., Huber, S., Bauer, U., Kwitt, R.: A stable multi-scale kernel for topological machine learning . In: 2015 IEEE Conference on Computer Vision and Pattern Recognition (CVPR), pp. 4741–4748. IEEE Computer Society, Los Alamitos, CA, USA (2015). <https://doi.org/10.1109/CVPR.2015.7299106> . <https://doi.ieeecomputersociety.org/10.1109/CVPR.2015.7299106>

Rabin, J., Peyré, G., Delon, J., Bernot, M.: Wasserstein barycenter and its application to texture mixing. In: International Conference on Scale Space and Variational Methods in Computer Vision, pp. 435–446 (2011). Springer

Santambrogio, F.: Optimal Transport for Applied Mathematicians, (2015)

Skraba, P., Turner, K.: Wasserstein stability for persistence diagrams. arXiv preprint arXiv:2006.16824 (2020)

Saadatfar, M., Takeuchi, H., Robins, V., Francois, N., Hiraoka, Y.: Pore Configuration Landscape of Granular Crystallization. *Nature Communications* **8**(1), 15082 (2017)

Tierny, J., Favelier, G., Levine, J.A., Gueunet, C., Michaux, M.: The Topology Toolkit. *IEEE transactions on visualization and computer graphics* **24**(1), 832–842 (2017)

Turner, K., Mileyko, Y., Mukherjee, S., Harer, J.: Fréchet means for distributions of persistence diagrams. *Discrete & Computational Geometry* **52**(1), 44–70 (2014) <https://doi.org/10.1007/s00454-014-9604-7> . Accessed 2025-03-24

Turner, K., Spreemann, G.: Same but different: Distance correlations between topological summaries. In: Baas, N.A., Carlsson, G.E., Quick, G., Szymik, M., Thaule, M. (eds.) *Topological Data Analysis*, pp. 459–490 (2020)

Wu, W., Kim, J., Rinaldo, A.: On the estimation of persistence intensity functions and linear representations of persistence diagrams. In: International Conference on

Artificial Intelligence and Statistics, pp. 3610–3618 (2024). PMLR

Wells, J.H., Williams, L.R.: Embeddings and Extensions in Analysis, (1975)

Xi, J., Niles-Weed, J.: Distributional convergence of the sliced wasserstein process.
Advances in Neural Information Processing Systems **35**, 13961–13973 (2022)

A Sliced Figalli–Gigli distance with a continuous projection

As mentioned in 5, we can change the projection we use in the definition of the SFG_p distance. In particular, the projection $z \mapsto \pi_t(z)$ is not continuous which motivates the introduction of *continuous versions* of our constructions. We hoped that this increased regularity would lead to better theoretical guarantees but we did not manage to obtain any. For the sake of completeness, we still present here our results on the continuous SFG distance.

Definition 4 (Continuous projections and the continuous SFG distance) Let $t \in \mathbb{R}$ et $z = (z_1, z_2) \in \Omega$, the *continuous* projection on the geodesic with parameter t is given by:

$$\tilde{\pi}_t(z) = \begin{cases} (t, t) + \frac{z_2 - z_1}{2}(1 - \frac{\|z - \pi_t(z)\|}{\|z - \pi(z)\|})(-1, 1) & \text{if } z_1 \leq t \leq z_2 \\ \partial\Omega & \text{otherwise.} \end{cases} \quad (104)$$

The continuous SFG distance is defined for $\mu, \nu \in \mathcal{M}^p(\Omega)$ as:

$$\widehat{\text{SFG}}_p(\mu, \nu) := \frac{p+1}{\sqrt{2}} \left(\int_{\mathbb{R}} \text{FG}_p^p(\tilde{\pi}_t \# \tilde{\mu}, \tilde{\pi}_t \# \tilde{\nu}) dt \right)^{\frac{1}{p}}. \quad (\widehat{\text{SFG}}_p)$$

This distance is also well-defined, following a computation similar to that of (SFG_p) .

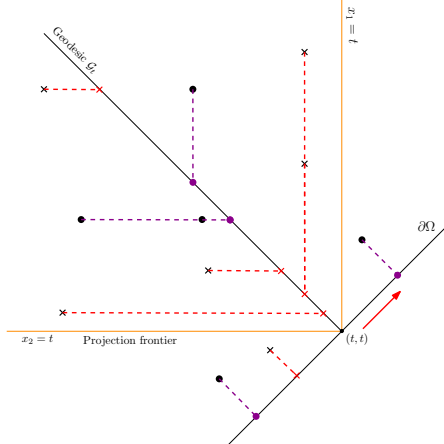


Fig. 8: Continuous projection

Proposition 14 Let $\mu \in \mathcal{M}^p(\Omega)$, and \emptyset denote the empty diagram. One has

$$\widehat{\text{SFG}}_p(\mu, \emptyset) = \text{FG}_p(\mu, \emptyset) = \text{Pers}_p(\mu). \quad (105)$$

Proof The proof is similar to that of Proposition 3. \square

We now prove that $\widehat{\text{SFG}}$ is a distance on the space of persistence diagrams $\mathcal{D}^p(\Omega)$. Extending the result to $\mathcal{M}^p(\Omega)$ as we did for SFG —which essentially boils down to prove injectivity of the corresponding transform—would require to adapt the proof technique of Proposition 4. It raises several challenges as the sublevel sets of that projection are not translation invariant. We left this possible extension for future work.

Proposition 15 $\widehat{\text{SFG}}_p$ is a distance on $\mathcal{D}^p(\Omega)$

Proof Let $\mu, \nu \in \mathcal{D}^p(\Omega)$ such that $\mu \neq \nu$ and define :

$$A = \{x \in \text{spt}(\mu) \cup \text{spt}(\nu) : d(x, \partial\Omega) = \max(\text{Pers}_\infty(\mu), \text{Pers}_\infty(\nu)) \text{ and } \mu(x) \neq \nu(x)\}$$

Observe that A is finite since we consider diagrams with finite persistence. Let $x \in A$ be such that x_2 is maximal and assume without loss of generality that $x \in \text{spt}(\mu)$ and $\mu(x) > \nu(x)$. Then, there exists $\varepsilon > 0$ such that for all $t \in I := [\frac{x_1+x_2}{2} - \varepsilon, \frac{x_1+x_2}{2} + \varepsilon[, \pi_t \# \tilde{\mu}(x) > \pi_t \# \tilde{\nu}(x)$ and therefore $\text{FG}_p(\tilde{\pi}_t \# \tilde{\mu}, \tilde{\pi}_t \# \tilde{\nu}) > 0$. Since $|I| > 0$, we also deduce that $\widehat{\text{SFG}}_p(\mu, \nu) \neq 0$. \square

Stability of $\widehat{\text{SFG}}$. Similarly to what was done for SFG_p we prove that $\widehat{\text{SFG}}_p$ is stable with respect to FG_p . We obtain the following:

Proposition 16 Let $\mu, \nu \in \mathcal{M}^p(\Omega) \cap \mathcal{M}^\infty(\Omega)$ one has:

$$\widehat{\text{SFG}}_p^p(\mu, \nu) \leq \sqrt{2}^p (p+2) \text{FG}_p^p(\mu, \nu) + M^{p-1} \iint_{\Omega \times \Omega} d(x, y) d\gamma(x, y), \quad (106)$$

where $M = \max(\text{Pers}_\infty(\mu), \text{Pers}_\infty(\nu))$.

Remark 10 In the case of $p = 1$, it is not necessary to suppose that μ and ν are in $\mathcal{M}^\infty(\Omega)$ and the above inequality becomes:

$$\forall \mu, \nu \in \mathcal{M}^1(\Omega), \widehat{\text{SFG}}_1(\mu, \nu) \leq (3\sqrt{2} + 1) \text{FG}_1(\mu, \nu). \quad (107)$$

Before proving 16, we first need a few straightforward results about the projections $\tilde{\pi}_t$. Let $x, y \in \Omega$ and $t \in \mathbb{R}$, we distinguish two cases: If $x_1 \leq t \leq x_2$ and $y_1 \leq t \leq y_2$:

$$\|\tilde{\pi}_t(x) - \tilde{\pi}_t(y)\| = \begin{cases} \sqrt{2}|y_1 - x_1| & \text{if } t \leq \frac{x_1+x_2}{2} \text{ and } t \leq \frac{y_1+y_2}{2} \\ \sqrt{2}|y_2 - x_2| & \text{if } t \geq \frac{x_1+x_2}{2} \text{ and } t \geq \frac{y_1+y_2}{2} \\ \sqrt{2}|y_1 + x_2 - 2t| & \text{if } \frac{x_1+x_2}{2} \leq t \leq \frac{y_1+y_2}{2} \\ \sqrt{2}|y_2 + x_1 - 2t| & \text{if } \frac{y_1+y_2}{2} \leq t \leq \frac{x_1+x_2}{2} \end{cases} \quad (108)$$

$$\leq \sqrt{2}\|x - y\| \quad (109)$$

If $y_1 \leq t \leq y_2$ and $t \notin [x_1, x_2]$:

$$\|\tilde{\pi}_t(x) - \tilde{\pi}_t(y)\| = \begin{cases} \sqrt{2}(t - y_1) & \text{if } t \leq \frac{y_1 + y_2}{2} \\ \sqrt{2}(y_2 - t) & \text{if } t \geq \frac{y_1 + y_2}{2} \end{cases} \quad (110)$$

From this, we deduce:

Lemma 7

$$\int_{\mathbb{R}} d(\tilde{\pi}_t(x), \tilde{\pi}_t(y))^p dt \leq \sqrt{2}^p \left(\frac{\sqrt{2}}{p+1} + \sqrt{2} \right) \max(d(x, \partial\Omega), d(y, \partial\Omega)) \|x - y\|^p. \quad (111)$$

Proof Suppose that $x_1 \leq y_1 \leq x_2 \leq y_2$, we then get:

$$\int_{\mathbb{R}} d(\tilde{\pi}_t(x), \tilde{\pi}_t(y))^p dt = \int_{x_1}^{y_1} \|\tilde{\pi}_t(x) - \pi(\tilde{\pi}_t(x))\|^p dt + \int_{y_1}^{x_2} \|\tilde{\pi}_t(x) - \tilde{\pi}_t(y)\|^p dt \quad (112)$$

$$+ \int_{x_2}^{y_2} \|\tilde{\pi}_t(y) - \pi(\tilde{\pi}_t(y))\|^p dt. \quad (113)$$

Using the results above, if $y_1 \leq \frac{x_1 + x_2}{2}$ we have

$$\int_{x_1}^{y_1} \|\tilde{\pi}_t(x) - \pi(\tilde{\pi}_t(x))\|^p dt = \int_{x_1}^{y_1} [\sqrt{2}(t - x_1)]^p dt \quad (114)$$

$$= \frac{\sqrt{2}^p}{p+1} (y_1 - x_1)^{p+1} \leq \frac{\sqrt{2}^p}{p+1} (x_2 - x_1) (y_1 - x_1)^p, \quad (115)$$

and if $y_1 \geq \frac{x_1 + x_2}{2}$ we have

$$\int_{x_1}^{y_1} \|\tilde{\pi}_t(x) - \pi(\tilde{\pi}_t(x))\|^p dt = \frac{\sqrt{2}^p}{p+1} \left(\frac{x_2 - x_1}{2} \right)^{p+1} + \int_{\frac{x_1 + x_2}{2}}^{y_1} [\sqrt{2}(x_2 - t)]^p dt \quad (116)$$

$$\leq \frac{\sqrt{2}^p}{p+1} (x_2 - x_1) (y_1 - x_1)^p. \quad (117)$$

Similarly,

$$\int_{x_2}^{y_2} \|\tilde{\pi}_t(y) - \pi(\tilde{\pi}_t(y))\|^p dt \leq \frac{\sqrt{2}^p}{p+1} (y_2 - y_1) (y_2 - x_2)^p. \quad (118)$$

Furthermore, using the results above we get: $\int_{y_1}^{x_2} \|\tilde{\pi}_t(x) - \tilde{\pi}_t(y)\|^p dt \leq \sqrt{2}^p (x_2 - x_1) \|x - y\|^p$ from which we deduce the desired result. The calculation is the same when $x_1 \leq y_1 \leq y_2 \leq x_2$. \square

Then, let γ be the optimal transport plan achieving the infimum in $\text{FG}_p(\mu, \nu)$. We can then define $\tilde{\gamma} \in \text{Adm}(\tilde{\mu}, \tilde{\nu})$ using Proposition 9, yielding the following result.

Proposition 17 *It holds that*

$$\int_{\mathbb{R}} \iint_{\Omega \times \Omega} d(\tilde{\pi}_t(x), \tilde{\pi}_t(y))^p d\tilde{\gamma}(x, y) dt \leq \sqrt{2}^{p+1} \left(1 + \frac{1}{p+1} \right) \iint_{\Omega \times \Omega} \|x - y\|^p d\gamma(x, y). \quad (119)$$

Proof Observe that $\text{spt}(\gamma) \cap \{(x, y) \in \Omega^2 : x_1 \leq x_2 \leq y_1 \leq y_2 \text{ or } y_1 \leq y_2 \leq x_1 \leq x_2\} = \emptyset$, the result is then a consequence of Lemma 7 and of the definition of $\tilde{\gamma}$. \square

We can then write:

$$\int_{\mathbb{R}} \iint_{\Omega \times \partial\Omega} d(\tilde{\pi}_t(x), \tilde{\pi}_t(y)) d\tilde{\gamma}(x, y) dt = \frac{\sqrt{2}}{p+1} \iint_{\Omega \times \partial\Omega} d(x, \partial\Omega)^{p+1} \frac{d\gamma(x, y)}{d(x, \partial\Omega)} \quad (120)$$

$$+ \frac{\sqrt{2}}{p+1} \iint_{\Omega_{1,+}} d(x, \partial\Omega)^{p+1} \left(\frac{1}{d(x, \partial\Omega)} - \frac{1}{d(y, \partial\Omega)} \right) d\gamma(x, y) \quad (121)$$

And:

$$\int_{\mathbb{R}} \iint_{\partial\Omega \times \Omega} d(\tilde{\pi}_t(x), \tilde{\pi}_t(y)) d\tilde{\gamma}(x, y) dt = \frac{\sqrt{2}}{p+1} \iint_{\partial\Omega \times \Omega} d(y, \partial\Omega)^{p+1} \frac{d\gamma(x, y)}{d(y, \partial\Omega)} \quad (122)$$

$$+ \frac{\sqrt{2}}{p+1} \iint_{\Omega_{2,+}} d(y, \partial\Omega)^{p+1} \left(\frac{1}{d(y, \partial\Omega)} - \frac{1}{d(x, \partial\Omega)} \right) d\gamma(x, y) \quad (123)$$

Where $\Omega_{1,+} = \{(x, y) \in \Omega \times \Omega : d(y, \partial\Omega) \geq d(x, \partial\Omega)\}$ and $\Omega_{2,+} = \{(x, y) \in \Omega \times \Omega : d(x, \partial\Omega) \geq d(y, \partial\Omega)\}$. Combining this with Proposition 17 we get:

$$\begin{aligned} \frac{\sqrt{2}}{p+1} \widehat{\text{SFG}}_p^p(\mu, \nu) &\leq \frac{\sqrt{2}^{p+1}}{p+1} \text{FG}_p^p(\mu, \nu) + \sqrt{2}^{p+1} \iint_{\Omega \times \Omega} d(x, y)^p d\gamma(x, y) \\ &\quad + \frac{\sqrt{2}}{p+1} \iint_{\Omega \times \Omega} \frac{\min(d(x, \partial\Omega), d(y, \partial\Omega))^p}{\max(d(x, \partial\Omega), d(y, \partial\Omega))} d(x, y) d\gamma(x, y) \end{aligned} \quad (124)$$

And, if we further suppose that $\mu, \nu \in \mathcal{M}^\infty(\Omega)$ we finally obtain the result of 16.

As in the case of SFG, a uniform lower bound is not obtainable for $\widehat{\text{SFG}}$. This time, the diagrams to consider are $\mu = \bigcup_{n=1}^p \{(-\alpha + 2n\delta, \alpha), (-\alpha + (2n+1)\delta, \alpha + \delta)\}$ and $\nu = \bigcup_{n=1}^p \{(-\alpha + 2n\delta, \alpha + \delta), (-\alpha + (2n+1)\delta, \alpha)\}$. One can then show that $\widehat{\text{SFG}}(\mu, \nu)$ is on the order of δ^{p+1} when $\text{FG}(\mu, \nu)$ is on the order of δ^p .

Topological equivalence of $\widehat{\text{SFG}}$ and FG. We proceed in the same way as for SFG to show that convergence for FG_p implies convergence for $\widehat{\text{SFG}}_p$.

Proposition 18 *Let $\mu \in \mathcal{D}^p(\Omega)$ and (μ_n) be a sequence of $\mathcal{D}^p(\Omega)$ such that $\mu_n \xrightarrow{\text{FG}_p} \mu$ then $\mu_n \xrightarrow{\widehat{\text{SFG}}_p} 0$.*

To prove the converse implication we will again show that convergence for $\widehat{\text{SFG}}$ implies characterisation (80). Like previously, we easily get the convergence of persistences:

Proposition 19 Let $\mu \in \mathcal{D}^p(\Omega)$ and (μ_n) be a sequence of $\mathcal{D}^p(\Omega)$ such that $\mu_n \xrightarrow{\text{SW}_p} \mu$. Then $\text{Pers}_p(\mu_n) \rightarrow \text{Pers}_p(\mu)$.

Proof We have $\widehat{\text{SW}}_p(\nu, \emptyset) = \text{Pers}_p(\nu)$ for all $\nu \in \mathcal{M}^p(\Omega)$. The result then follows from the triangle inequality. \square

In order to prove that the $\widehat{\text{SFG}}_p$ convergence implies vague convergence we will proceed in a similar manner as for SFG by simply changing the shape of the region B_ε .

Definition 5 We now denote by $\hat{B}_{\varepsilon,t}$ the "elbow" of width ε centered at $x + (t - t_x)(1, 1)$ where $t_x = \frac{x_1 + x_2}{2}$ (see Figure 3). We denote by $\hat{B}_{\varepsilon,v,t}$ (resp. $\hat{B}_{\varepsilon,h,t}$) the vertical (resp. horizontal) part of $\hat{B}_{\varepsilon,t}$. We also define the following quantity (similar to $\tilde{\text{SFG}}$):

$$\bar{\text{SFG}}_{\varepsilon,\eta}(\mu, \nu) := \frac{1}{\sqrt{2}} \left(\int_{\mathbb{R}} \tilde{\text{FG}}_{B_{\varepsilon,t}, B_{\eta,t}}^p(\tilde{\pi}_t \# \tilde{\mu}, \tilde{\pi}_t \# \tilde{\nu}) dt \right)^{\frac{1}{p}}. \quad (125)$$

As before, we also define $\Delta_{t,\varepsilon} := \tilde{\mu}_n(B_{\varepsilon,t}) - \tilde{\mu}(B_{\varepsilon,t})$, $\Delta_{v,t,\varepsilon} = \tilde{\mu}_n(B_{\varepsilon,v,t}) - \tilde{\mu}(B_{\varepsilon,v,t})$ and $\Delta_{h,t,\varepsilon} = \tilde{\mu}_n(B_{\varepsilon,h,t}) - \tilde{\mu}(B_{\varepsilon,h,t})$.

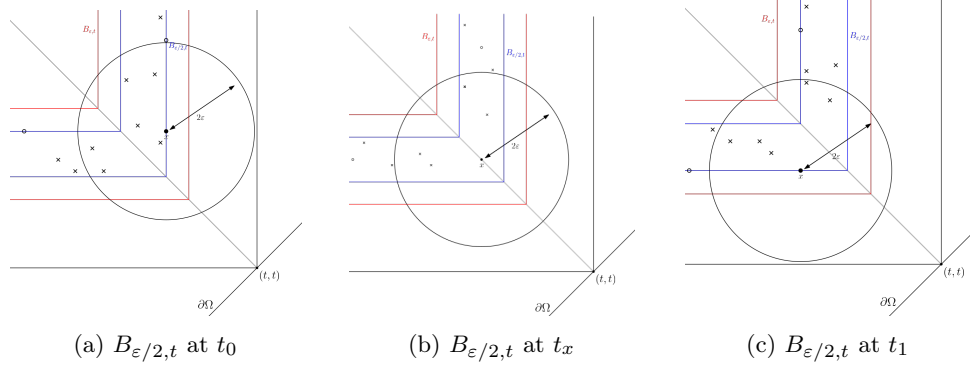


Fig. 9: The construction we use for the proof of Proposition 12. $B_{\varepsilon,t}$ is in red, $B_{\varepsilon/2,t}$ is in blue. Points of μ_n are represented by crosses, and those of μ by circles. ε was chosen small enough so that all circles lie on $D_{x,v} \cup D_{x,h}$

With these new definitions, the results of Lemmas 5 and 6 still hold. The proof is then very similar to that of Proposition 12, we argue by contradiction to lower bound $\bar{\text{SFG}}$ by studying Δ_t , $\Delta_{v,t}$ and $\Delta_{h,t}$.

Proposition 20 Let $\mu \in \mathcal{D}^p(\Omega)$ and (μ_n) a sequence of $\mathcal{D}^p(\Omega)$ satisfying $\mu_n \xrightarrow{\widehat{\text{SW}}_p} \mu$. Then, for all $x \in \text{spt}(\mu)$, there exists $\eta > 0$ such that for any $0 < \varepsilon < \eta$, $\mu_n(1_{B(x,\varepsilon)}) \rightarrow \mu(x)$

Proof We again argue by contradiction and assume there exists a point x such that for all $\eta > 0$, there exists $\varepsilon > 0$ verifying $\mu_n(1_{B(x, 2\varepsilon)}) \neq \mu(x)$ for infinitely many n . We denote by t_0 the instant at which x appears in $B_{\varepsilon/2, t}$ and t_1 the instant at which it disappears. We also set $B_{\varepsilon, x} := \bigcup_{t \in [t_0, t_1]} B_{\varepsilon, t}$. Similarly to what we did before, we can reduce ε so that the only points of $\text{spt}(\mu) \cap B_{\varepsilon, x}$ are contained in $D_{x, v} = \{y \in \Omega : y_1 = x_1 \text{ and } y_2 > x_2\}$ or $D_{x, h} = \{y \in \Omega : y_2 = x_2 \text{ and } y_1 < x_1\}$. We will now lower bound $\widehat{\text{SFG}}_{\varepsilon/2, \varepsilon}(\mu_n, \mu)$ to obtain a contradiction.

First, there cannot be $y \in \text{spt}(\mu_n)$ verifying $d(y, \partial\Omega) > \text{Pers}_\infty(\mu) + 1$ or we would have $\widehat{\text{SFG}}(\mu_n, \mu) > \frac{C}{\text{Pers}_\infty(\mu) + 1}$. Lastly any point appearing in $B_{\varepsilon/2, t}$ between t_0 and t_1 cannot disappear in that same time frame. As such, we deduce that at most $K := (\text{Pers}_\infty(\mu) + 1)(\mu(B_\varepsilon) + 1)$ points of μ_n appear in $B_{\varepsilon/2, t}$ between t_0 et t_1 .

We will now show that we cannot have $\Delta_{v, t} > \varepsilon/8$ or $\Delta_{h, t} > \varepsilon/8$ for a duration longer than $\varepsilon/8$. For this, we need the following lemma

Lemma 8 *Let $t_1 < t_2 \in \mathbb{R}$, $x \in B_{\varepsilon, h, t_1}$ and $y \in B_{\varepsilon, v, t_2}$ then:*

$$\int_{t_1}^{t_2} d(\tilde{\pi}_t(x), \tilde{\pi}_t(y)) dt \geq (t_2 - t_1)^2. \quad (126)$$

Proof We denote $x = (x_1, x_2)$ and $y = (y_1, y_2)$. We have

$$\int_{t_1}^{t_2} d(\tilde{\pi}_t(x), \tilde{\pi}_t(y)) dt = 2 \int_{t_1}^{t_2} |x_1 + y_2 - 2t| dt \quad (127)$$

$$\geq 2 \left[(t_1 - \frac{x_1 + y_2}{2})^2 + (t_2 - \frac{x_1 + y_2}{2})^2 \right] \quad (128)$$

$$\geq (t_2 - t_1)^2 \quad (129)$$

□

Suppose now for a contradiction that there exists $\alpha \in \mathbb{R}$ such that $\Delta_{v, t} > \varepsilon/8$ or $\Delta_{h, t} > \varepsilon/8$ for all $t \in [\alpha, \alpha + \varepsilon/8]$. Observe that the optimal transport plan $\pi_{n, t}$ from $\pi_t \# \tilde{\mu}_n$ to $\pi_t \# \tilde{\mu}$ only changes in finitely many instants $t \in [\alpha, \alpha + \varepsilon/8]$: those where a point of μ_n and a point of μ have the same projection under π_t and those where a point of μ_n disappears/appears in $B_{\varepsilon/2, t}$. This can happen at most $4K$ times. Thus, there exists $\alpha = t_1 \leq \dots \leq t_{4K} = \alpha + \varepsilon/8$ such that for all $1 \leq i \leq 4K$ and all $t \in [t_i, t_{i+1}]$ we have $\pi_{n, t} = \pi_{n, t_i}$. Furthermore, since we are supposing that $\Delta_{v, t} > \varepsilon/8$ or $\Delta_{h, t} > \varepsilon/8$, we get the existence of $A_t \subset B_{\varepsilon/2, t, h} \times B_{\varepsilon/2, t, v} \cup B_{\varepsilon/2, t, v} \times B_{\varepsilon/2, t, h}$ and $C_t \subset B_{\varepsilon/2, t} \times \partial B_{\varepsilon, t} \cup \partial B_{\varepsilon/2, t} \times (D_{x, v} \cup D_{x, h})$ such that $\pi_{n, t}(A_t \cup C_t) > \varepsilon/8$ for all $t \in [\alpha, \alpha + \varepsilon/8]$. We can then write:

$$\int_{\alpha}^{\alpha + \varepsilon/8} \iint_{\overline{B_{\varepsilon/2, t} \times B_{\varepsilon/2, t}}} d(\tilde{\pi}_t(x), \tilde{\pi}_t(y)) d\pi_{n, t}(x, y) dt \quad (130)$$

$$= \sum_{i=1}^{4K} \int_{t_i}^{t_{i+1}} \iint_{\overline{B_{\varepsilon/2, t} \times B_{\varepsilon/2, t}}} d(\tilde{\pi}_t(x), \tilde{\pi}_t(y)) d\pi_{n, t_i}(x, y) dt \quad (131)$$

$$\geq \sum_{i=1}^{4K} \iint_{A_{t_i} \cup C_{t_i}} \int_{t_i}^{t_{i+1}} d(\tilde{\pi}_t(x), \tilde{\pi}_t(y)) dt d\pi_{n, t_i}(x, y) \quad (132)$$

$$\begin{aligned}
&\geq \sum_{i=1}^{4K} \pi_{n,t_i}(A_{t_i})(t_{i+1} - t_i)^2 + \pi_{n,t_i}(C_{t_i}) \times \varepsilon/2 \\
&\quad \text{(according to Lemma 8)} \\
&\geq \frac{\varepsilon}{8} \times \frac{(\varepsilon/8)^2}{4K} \quad \text{(by possibly reducing } \varepsilon \text{ below 1)}
\end{aligned}$$

As such we cannot have $\Delta_{v,t} > \varepsilon/8$ or $\Delta_{h,t} > \varepsilon/8$ for longer than $\varepsilon/8$. However at the instant $t_x = \frac{x_1+x_2}{2}$, the point x of multiplicity $\mu(x)$ goes from $B_{\varepsilon/2,v}$ to $B_{\varepsilon/2,h}$ whereas between $t_x - \varepsilon/2$ and $t_x + \varepsilon/2$, $r \neq \mu(x)$ points of μ_n go from $B_{\varepsilon/2,v}$ to $B_{\varepsilon/2,h}$. As such, around t_x , at least one point of μ_n must disappear in $B_{\varepsilon/2,v}$ and appear in $B_{\varepsilon/2,h}$ (or the other way around). But then, this would imply that $\Delta_{3\varepsilon/4,t} > \frac{3}{4(\text{Pers}_\infty(\mu)+1)}$ for a duration at least $\varepsilon/4$, and thus we would get $\text{SFG} \geq \frac{3\varepsilon^2}{32(\text{Pers}_\infty(\mu)+1)}$ which yields the desired contradiction. \square